Research Article

Nano Research
2023, 16(1): 792–809

ISSN 1998-0124 CN 11-5974/O4
https://doi.org/10.1007/s12274-022-4670-2

Soft nanofiber modified micropatterned substrates enhance native-like endothelium maturation via CXCR4/calcium-mediated actin cytoskeleton assembly

Bingcheng Yi[1,2], Boya Zhou[2], Wufei Dai[2], Xinwu Lu[1], and Wei Liu[2] (✉)

[1] *Department of Vascular Surgery, Shanghai Ninth People's Hospital, Shanghai Jiao Tong University School of Medicine, Shanghai 200011, China*
[2] *Department of Plastic and Reconstructive Surgery, Shanghai Key Laboratory of Tissue Engineering, Shanghai Ninth People's Hospital, Shanghai Jiao Tong University School of Medicine, Shanghai 200011, China*

Received: 28 April 2022 / **Revised:** 11 June 2022 / **Accepted:** 16 June 2022

ABSTRACT

Regeneration and maturation of native-like endothelium is crucial for material-guided small-diameter vascular regeneration. Although parallel-microgroove-patterned (micropatterned) substrates are capable of promoting endothelial regeneration with native-like endothelial cell (EC) alignment, their unbefitting high-stiffness acutely inhibits cell–matrix interaction and endothelial maturation. Given that the sufficient softness of nanofibers allows cells to deform the local matrix architecture to satisfy cell survival and functional requirements, in this study, an effective strategy of decorating micropatterned substrate with soft nanofibers was exploited to enhance cell–matrix interaction for engineering healthy endothelium. Results demonstrated that the micropatterned nanofibrous membranes were successfully obtained with high-resolution parallel microgrooves (groove width: ~ 15 μm; groove depth: ~ 5 μm) and adequate softness (bulk modulus: 2.27 ± 0.18 MPa). This particular substrate markedly accelerated the formation and maturation of confluent native-like endothelium by synchronously increasing cell–cell and cell–matrix interactions. Transcriptome analysis revealed that compared with smooth features, the microgrooved pattern was likely to promote endothelial remodeling via integrin α5-mediated microtubule disassembly and type I interleukin 1 receptor-mediated signaling pathways, whereas the nanofibrous pattern was likely to guide endothelial regeneration via integrin α5β8-guided actin cytoskeleton remodeling. Nevertheless, endowing micropatterned substrate with soft nanofibers was demonstrated to accelerate endothelial maturation via chemokine (C-X-C motif) receptor 4/calcium-mediated actin cytoskeleton assembly. Furthermore, numerical simulation results of hemodynamics indicated the positive impact of the micropatterned nanofibers on maintaining stable hemodynamics. Summarily, our current work supports an affirmation that the micropatterned nanofibrous substrates can significantly promote regeneration and maturation of native-like endothelium, which provides an innovative method for constructing vascular grafts with functional endothelium.

KEYWORDS

small-diameter vascular grafts, parallel microgrooves, nanofibers, cell–matrix interaction, endothelial regeneration

1 Introduction

The endothelium, an oriented endothelial cell (EC) monolayer between the blood and blood vessel wall, acts as a selective barrier to finely tune vascular homeostasis. Loss of endothelial barrier function has been implicated in a variety of vascular diseases, such as thrombosis, atherosclerosis, and intimal hyperplasia [1, 2]. Recently, tissue-engineered vascular grafts (TEVGs) are proposed as promising alternative to achieve functional recovery of diseased vascular tissues, especially for the case of small-diameter (inner diameter < 4 mm) blood vessels [3–5]. However, incomplete endothelialization or dysfunction of the regenerated endothelial monolayer on the inner surface of TEVGs have been frequently observed to cause acute post-implantation complications [5, 6]. Hence, over the past years, great attention and effort have been made to achieve rapid endothelialization through surface modification techniques including immobilization of biomolecules (e.g., cell-capturing molecules [7], growth factors [8], and therapeutic genes [9]). Nonetheless, dysfunction of regenerated endothelium remained observable during TEVG-mediated vascular regeneration [2, 10]. Such evidence supports and verifies the fact that fully regenerated EC monolayer is not necessarily synonymous with full restoration of healthy endothelial function. In this context, the precise design of TEVG surface and interface signals will be a critical factor for improving endothelial function of the regenerated endothelium in order to develop promising alternatives to blood vessels. Yet, it remains a great challenge in this field thus far.

In natural blood vessels, the overall integrity and function of the endothelium are governed by three main categories of inputs: cell–cell and cell–matrix interactions, soluble mediators (e.g., thrombin and nitric oxide), and biomechanics (e.g., fluid shear stress and stretch) [11]. Inspired by these inputs, one can envision that increasing cell–cell and cell–substrate interactions will be an inherent requirement for endothelial regeneration and its

Address correspondence to liuwei_2000@yahoo.com

functional remodeling. As demonstrated in our recent work, lysine-doped polydopamine modified substrates significantly promoted the formation and maturity of compact endothelial monolayer via concurrent enhancement of cell–cell and cell–substrate interactions [12]. However, so far, little attention has been paid on increasing cell–cell and cell–substrate interactions by precisely designing the substrate structural cues, which has been also deemed as a key regulatory factor in controlling structural integrity and integrated remodeling of TEVGs for enhanced vascular regeneration [13]. In view of the oriented morphology of native endothelium, the past efforts have provided insights into the surface topographic modification with line-shaped ridges and grooves in order to generate the native-like EC alignment on the substrates [14–16]. Such microgroove patterns are demonstrated able to effectively improve endothelial regeneration via enhancing cell–cell interaction [15]. However, from the aspect of mechanics-dependent cell-matrix communication, the parallel-microgroove-patterned (i.e., micropatterned) substrates are usually accompanied by an unbefitting high-stiffness, which makes the myosin-generated contractile forces exerted by cells hardly to modulate their surrounding microenvironment for cell requirements (Fig. 1(a)) [17]. Under the persistent impact of a force-feedback loop between matrix and cells [17], the reduced cell–matrix interaction will ulteriorly impede the healthy remodeling of a regenerated endothelium and thereby leads to considerable complications once applied to clinical translation. Based on these phenomena, we hypothesized that development of a functional TEVG, that not only favors the replication of structural anisotropy of endothelium, but also provides a suitable microenvironment for cell–matrix interaction, would be beneficial to healthy endothelial remodeling.

Native vascular extracellular matrix (ECM) is a complex network of fibrous biopolymers and interstitial space, which provides signals to guide local ECs to promote vascular tissue homeostasis and regeneration [18]. Inspired by this, nanofibrous substrates have been extensively used in engineering vascular tissues, attributing to their unique nano-/microscale fineness that closely resembles the fibrous pattern of ECM and provides high specific surface area for binding biomolecules [19, 20]. Meanwhile, their adequate softness also exhibits irreplaceable advantages for mediating cell–matrix interaction [21], which allow cells to exert force on the matrix surface and permit the cell-generated contractile forces to deform the local architectures for satisfying cellular requirement, thereby creating a self-adaptive microenvironment for complex cellular functions [22]. In this case, uses of aligned nanofibers are indeed of considerable interest and importance for constructing functional TEVGs, as they can positively regulate cell–matrix interaction for desired cell phenotypic switch and concurrently guide ECs to spread and align along fiber direction [2, 6, 12]. Regrettably, with the limitations of fiber structural instability upon shear flows, dense fiber accumulation, and inherent anisotropic mechanical properties, the aligned-nanofiber-constructed TEVGs were demonstrated to be less capable of guiding vascular regeneration *in vivo* [23]. To solve the problem, Shin et al. demonstrated that using femtosecond laser ablation to create microgrooves on random nanofibrous membrane could successfully regulate the morphology and biological function of ECs to resemble the native endothelium [23], but this strategy inevitably destroyed the structural integrity of nanofibrous membrane that was inappositely applied as blood-contacting grafts. Inspired by the aforementioned findings, we speculated that featuring a micropatterned substrate with random nanofibers (or namely "topologically modified nanofibrous platform with microgrooves"), aiming to enhance cell–matrix interaction under the contact guidance of parallel microgrooves, may provide a promising strategy to realize the successful engineering of healthy endothelium on graft surface (Fig. 1(b)).

To verify this hypothesis, precisely-designed micropatterned nanofibrous scaffold was fabricated by a simple and reproducible method of combined electrospinning and soft lithography in this

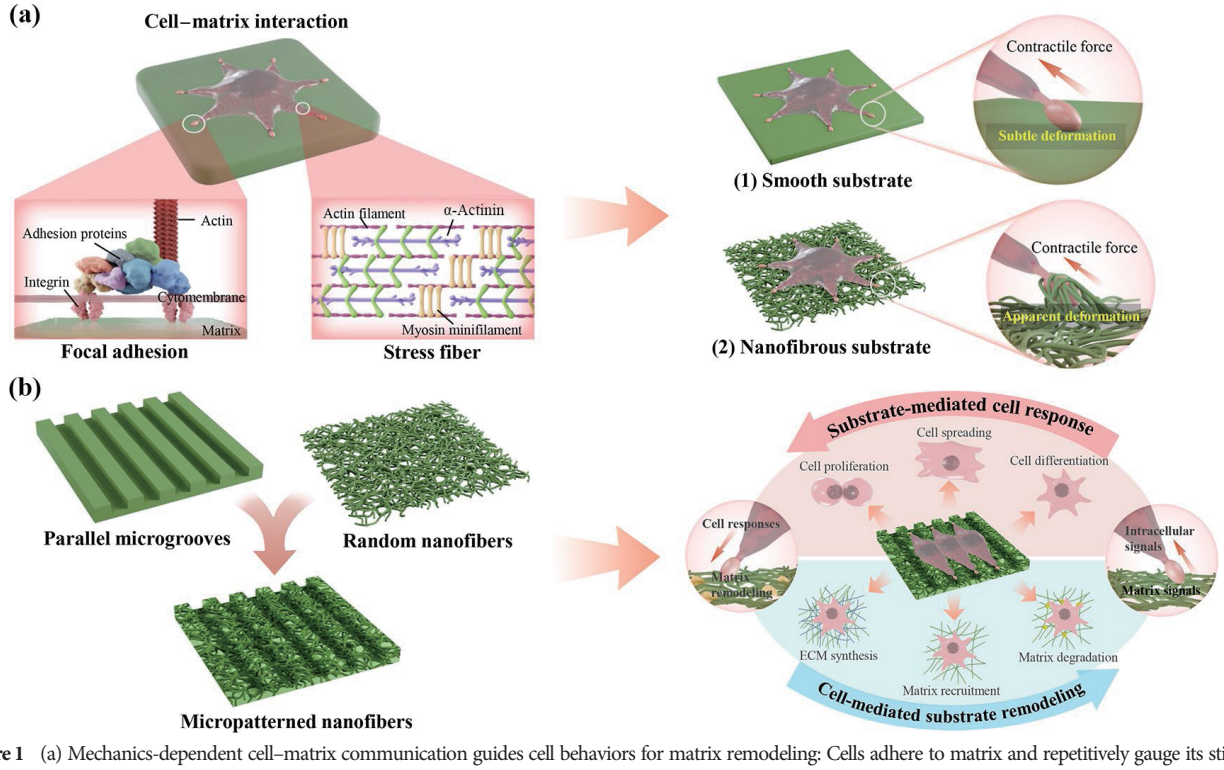

Figure 1 (a) Mechanics-dependent cell–matrix communication guides cell behaviors for matrix remodeling: Cells adhere to matrix and repetitively gauge its stiffness through focal adhesion, then transmit the sensed mechanical signals to the nucleus along stress fibers for cellular responses. Under this interactive process, comparing to the compact films, soft nanofibers are more propitious to permit cell-mediated matrix deformation for cell growth and vascular remodeling. (b) Hypothesis: Featuring the micropatterned film with soft nanofibers to enhance cell–matrix interaction may enhance EC functions and promote healthy endothelial remodeling.

study. After characterizations of surface patterns and mechanical properties, the effect of the obtained micropatterned nanofibers on inducing endothelial regeneration was assessed by analyzing cell morphology, cell–cell interaction, cell–matrix interaction, and the expression of specific EC markers. Thereafter, gene expression profile (GEP) analysis, differentially expressed genes (DEGs), and their biological implications were implemented to elucidate the underlying mechanisms involved in these topographic patterns mediated endothelial regeneration. Lastly, numerical simulation related to evolution of flow systems was performed to assess the effect of the substrate geometry parameters on hemodynamics, aiming to evaluate the potential uses of the micropatterned nanofibers for constructing TEVGs in proof-of-concept.

2 Experimental

2.1 Preparation of micropatterned nanofibers

2.1.1 Fabrication of the micropatterned PLCL nanofibers

Given that 20 μm parallel microgrooves were capable of inducing oriented EC monolayer formation via contact guidance [13, 23], the micropatterned poly (L-lactide-co-caprolactone) (PLCL) nanofibers were fabricated via electrospinning, with the silicon wafer featuring 20 μm width and 20 μm depth (Suzhou Cchip Scientific Instrument Co. Ltd., China) used as the element to collect nanofibers (Fig. S1 in the Electronic Supplementary Material (ESM)). Briefly, polymeric solution with a final concentration of 4% (w/v) was prepared by dissolving PLCL (LA/CL 50:50, IV 2.9 dl/g, Jinan Daigang Biomaterials, China) into 1,1,1,3,3,3-hexafluoro-2-propanol (HFIP, Chembee, China). After stirring for 12 h, the solution was electrospun to fabricate the micropatterned nanofibers (designated as F_G) under the following parameters: applied voltage of 13 kV, flow rate of 0.5 mL/h, needle tip to drum-collector gap distance of 18 cm, and ambient conditions of 20–25 °C and 25%–30% humidity. For the purpose of comparison, random nanofibers (designated as Fiber), micropatterned films (designated as Groove), and smooth films (designated as Smooth) were also prepared. For random nanofibers, smooth aluminum foil was used to collect nanofibers and electrospinning was performed according to the same parameters. To gain the micropatterned films, replica molding was performed with the silicon wafer that featured with 20 μm width and 6 μm depth to serve as a mold. In brief, PLCL solution was poured to cover the silicon wafer mold. After complete evaporation of HFIP, the mold was removed to obtain the micropatterned film. As for smooth and flat films, smooth glass was chosen as the mold to guide the formation of smooth patterns on substrate via replica molding. All the obtained samples were subjected to vacuum-drying for 2 weeks.

2.1.2 Characterizations of the micropatterned PLCL nanofibers

Surface microstructures and topographies. Surface microstructures of the obtained samples were characterized using a scanning electron microscope (SEM, Gemini 300, ZEISS). Prior to imaging, all samples were sputter-coated with gold for 30 s to increase conductivity. SEM images were then taken under the high vacuum mode at an acceleration voltage of 0.02–30 kV. Surface topographies of the obtained samples were evaluated using three-dimensional (3D) laser scanning microscope (VK-X3000, Keyence), and an area of 285 μm × 215 μm was scanned for all the samples to obtain the high profile of 3D images. To calculate the surface topographies, the cross-sectional linear scanning profiles were further measured.

Local and bulk mechanical properties. Local Young's modulus of the obtained samples was characterized using an atomic force microscope (AFM, NT-MDT Prima Dimension FastScan, Bruker). High-resolution maps showing modulus variations were taken at a scanning area of 10 μm × 10 μm using the AFM instrument. Bulk tensile properties of the obtained samples were further detected by a tabletop tensile tester (Instron, USA) under a stretching speed of 10 mm/min. Young's modulus and tensile strength were derived from the generated stress–strain curves. For each group, at least 8 samples were tested.

2.2 Assessments of the micropatterned PLCL nanofibers' effect on endothelial regeneration

2.2.1 Cell culture and seeding

Human umbilical vein endothelial cells (HUVECs) were purchased from ScienCell Research Laboratories and were cultured in a commercial, customized cell culture medium (human Endothelial Cell Medium, ScienCell, USA) that contains 5% fetal bovine serum (FBS), 1% penicillin/streptomycin, and 1% endothelial cell growth factor supplements. During cell culture of HUVECs, the medium was changed every 2 days. Prior to cell seeding, all samples were sterilized by ultraviolet light irradiation for 6 h followed by 75% ethanol treatment for 2 h. After 3 washes with phosphate-buffered saline (PBS), the sterilized samples were placed into 24- or 6-well culture plates and then pre-incubated with human endothelial cell medium overnight at 37 °C. When the cultured HUVECs (3–8 passages) reached 90% confluence, the cells were collected using trypsin-ethylenediaminetetraacetic acid (EDTA) and then seeded onto the treated samples.

2.2.2 Assessments of endothelial monolayer formation

Cell morphology in the EC monolayer. To analyze the effect of the micropatterned nanofibers on endothelial monolayer morphology, HUVECs were seeded onto different samples in 24-well plates at a high density of 3×10^5 cells/cm^2 for the formation of HUVEC monolayer. After culture of 3 days, actin cytoskeleton and cell nucleus of HUVEC monolayer were stained with TRITC Phalloidin (Yeasen Biotechnology, China) and 4',6-diamidino-2-phenylindole (DAPI, Yeasen Biotechnology, China), respectively. Briefly, the cellularized constructs were fixed using 4% paraformaldehyde (Biosharp, China) for 30 min and then permeabilized using 0.2% Triton X-100 (Solarbio, China) for 5 min. After 3 times of rinsing with PBS, the F-actin of HUVEC monolayer was stained with phalloidin (1:200 dilution) for 30 min followed by the counterstaining of cell nuclei with DAPI (1:1,000 dilution) for 10 min at room temperature in the dark. Subsequently, cell morphology was observed using a laser-scanning confocal microscopy (Carl Zeiss, Germany).

Cell-substrate interaction. The expression of integrin β1 in the focal adhesions (FAs) was performed to evaluate the ability of the micropatterned PLCL nanofibers to enhance cell–substrate interaction. HUVECs were seeded onto the samples in 24-well culture plates at a low density of 3×10^4 cells/cm^2, and then the integrin β1 expression of single HUVECs was analyzed using immunofluorescence staining after culturing for 3 days. Briefly, the cellularized constructs were fixed using 4% paraformaldehyde for 30 min, and then permeabilized with 0.2% Triton X-100 for 5 min, followed by the blocking using 10% goat serum (Solarbio, China) for 30 min. Thereafter, the constructs were incubated with rabbit anti-human integrin β1 polyclonal antibody (Proteintech, 1:200 dilution) overnight at 4 °C, and then incubated with fluorescein (FITC)-conjugated AffiniPure goat anti-rabbit immunoglobulin (IgG) (H + L) antibody (Proteintech, 1:50 dilution) for 90 min at room temperature. Finally, the cell nuclei

were counterstained with DAPI for 10 min, and the expression of integrin β1 was observed using laser-scanning confocal microscopy. For quantitative analysis of the averaged FA size, image analysis of integrin β1 was done by a focal adhesion analysis server [24, 25].

Cell proliferation. HUVECs were seeded onto the samples in 24-well plates at a high density of 3×10^5 cells/cm^2 for endothelial monolayer formation. After the culture of 1, 3, and 5 days, the cellularized constructs were incubated with 300 μL fresh human endothelial cell medium containing 5% cell counting kit (CCK)-8 (Beyotime, China) for 4 h at 37 °C. Thereafter, 100 μL of the solution was transferred into a 96-well plate for absorbance measurements at 450 nm using a microplate reader (MK3, Thermo, USA).

2.2.3 Function assessments of endothelial monolayer

Low-density lipoprotein uptake. HUVECs were seeded onto the samples in 24-well culture plates at a low density of 3×10^4 cells/cm^2. After 3 days of culture, the cellularized constructs were incubated with 450 μL fresh human endothelial cell medium containing 30 μg/mL DiI-labeled human acetylated low-density lipoprotein (Ac-LDL, Yeason, China) for 4 h at 37 °C. Then, the Ac-LDL uptake into HUVEC cytoplasm was observed under laser-scanning confocal microscopy at an excitation wavelength of 550 nm. For quantitative analysis, the fluorescence intensity of Ac-LDL images was examined using ImageJ software based on the obtained fluorescence images ($n > 8$), and was normalized to a single cell.

Endothelial monolayer maturity. The integrity and maturity of HUVEC monolayer formed on the micropatterned nanofibers was examined by VE-cadherin immunostaining (a cell–cell junction marker [12]). Briefly, HUVECs were seeded onto the samples in 24-well plates at a high density of 3×10^5 cells/cm^2 for confluent cell monolayer formation. After 3 days of culture, immunofluorescence staining was performed to detect the vascular endothelial (VE)-cadherin expression of HUVEC monolayer using rabbit anti-human VE-cadherin antibody (1:200 dilution, Bioss, China) followed by FITC-conjugated AffiniPure goat anti-rabbit IgG (H + L) (1:50 dilution). The detailed process was conducted following the protocol in Section 2.2.2. Finally, the constructs were observed using laser-scanning confocal microscopy, and the averaged thickness of cell–cell junction within the endothelial monolayer was measured from the obtained fluorescence images using ImageJ software.

2.3 Transcriptome analysis of micropatterned nanofibers mediated endothelialization

HUVECs were seeded onto the samples in 6-well plates at a high density of 3×10^5 cells/cm^2 to form a confluent cell monolayer. After 3 days of culture, the total ribonucleic acid (RNA) was extracted from HUVEC monolayer using Trizol reagent (Absin, China), and then were used to construct RNA sequencing libraries. After RNA sequencing mapping and DEG analysis, gene ontology (GO) analysis was performed to elucidate the biological implications of the DEGs. Detailed methods see the Electronic Supplementary Material (ESM).

2.4 Numerical simulation of hemodynamics on the micropatterned PLCL nanofibers

To assess the potential uses of the micropatterned nanofibers for constructing TEVGs, the effect of their surface topographic cues on hemodynamics was evaluated using mathematical modeling method. The numerical simulations were performed using Fluent 14.0 computational fluid dynamics (CFD) software (Ansys, USA). Four different geometry models were built according to surface scanning electron microscopy (SEM) images of the obtained samples. The velocity profiles of blood flowing through these topographic patterns were investigated, including the local velocity profiles on the surface regions of the samples and the global velocity profiles on the domains of the samples-formed tubes. After that, surface streamline and 3D streamline images were obtained from the numerical simulations. In all models, the inlet and the outlet conditions were specified by a constant blood density (1,050 kg/m^3) and viscosity (0.003 Pa·S). The initial flow direction was along the x-axis, and in the inlet (cross-section of the plate at $x = 0$) the velocity was constant.

2.5 Statistical analysis

All quantification data were presented as means ± standard deviation. The significant difference among multiple groups was detected with one-way ANOVA and then with Tukey's post hoc test used for pair-wise comparisons using the Origin 9.0 software. A value of $^*p < 0.05$ or $^{**}p < 0.01$ was considered statistically significant. All the experiments were carried out at least thrice.

3 Results

3.1 Micropatterned nanofibers exhibited anisotropic topographic features and adequate softness

PLCL was chosen as a model polymer for electrospinning in this study, attributing to its inherent excellent elasticity and widespread uses for constructing TEVGs [12, 26]. A combination of electrospinning and soft lithography technique was proven to be effective in realizing the topographic modification of random PLCL nanofibrous membrane with parallel microgroove patterns (Fig. 2). As proven in SEM results, the highly repeatable parallel microgroove patterns were successfully transferred from the micropatterned silicon wafer (as a collector for nanofiber deposition) onto the nanofibrous membranes (Fig. 2(a)). With the data of quantified fiber diameters (Fig. S2(a) in the ESM), no significant difference was detected between the micropatterned nanofibers and pure random nanofibers (F_G: 0.49 ± 0.08 μm vs. Fiber: 0.52 ± 0.12 μm). After visualizing the patterned surface of the samples and quantifying their surface topographies using 3D laser scanning microscopy, we found that the obtained F_G exhibited the features with an averaged groove width of 14.92 ± 1.56 μm (Fig. S2(b) in the ESM), and the pitch size did not vary significantly with locations (Fig. 2(b)). These data indicated a high degree of repeatability and good fidelity of this patterning process. However, groove depth of the parallel microgroove patterns changed significantly after topography replication, in which the groove depth of micropatterned nanofibers significantly reduced from 20 μm (mold size) to 5.16 ± 0.55 μm (Fig. 2(b) and Fig. S2(c) in the ESM). This was likely attributed to the internal stress resident within each of the nanofibers that hinders the nanofibers to reach the groove bottom during electrospinning [27]. To fabricate micropatterned films with the similar groove depth, the silicon wafer (groove width: 20 μm) featuring groove depth of 6 μm was used for replica molding. As expected, clear patterns of parallel microgroove were detected on the surface of micropatterned films (i.e., Groove), and no significant differences in groove width and groove depth were detected compared to micropatterned nanofibers (Figs. S2(b) and S2(c) in the ESM).

Because of the ECM-like ultrafine fineness, nanofibers have been demonstrated to exhibit a sufficiently lowered softness that enabled cells to play with them for efficacious remodeling [28]. As verified in Figs. 2(c) and 2(d), the local modulus of Groove was 1,174.53 ± 320.32 MPa whereas that of F_G was only 149.56 ±

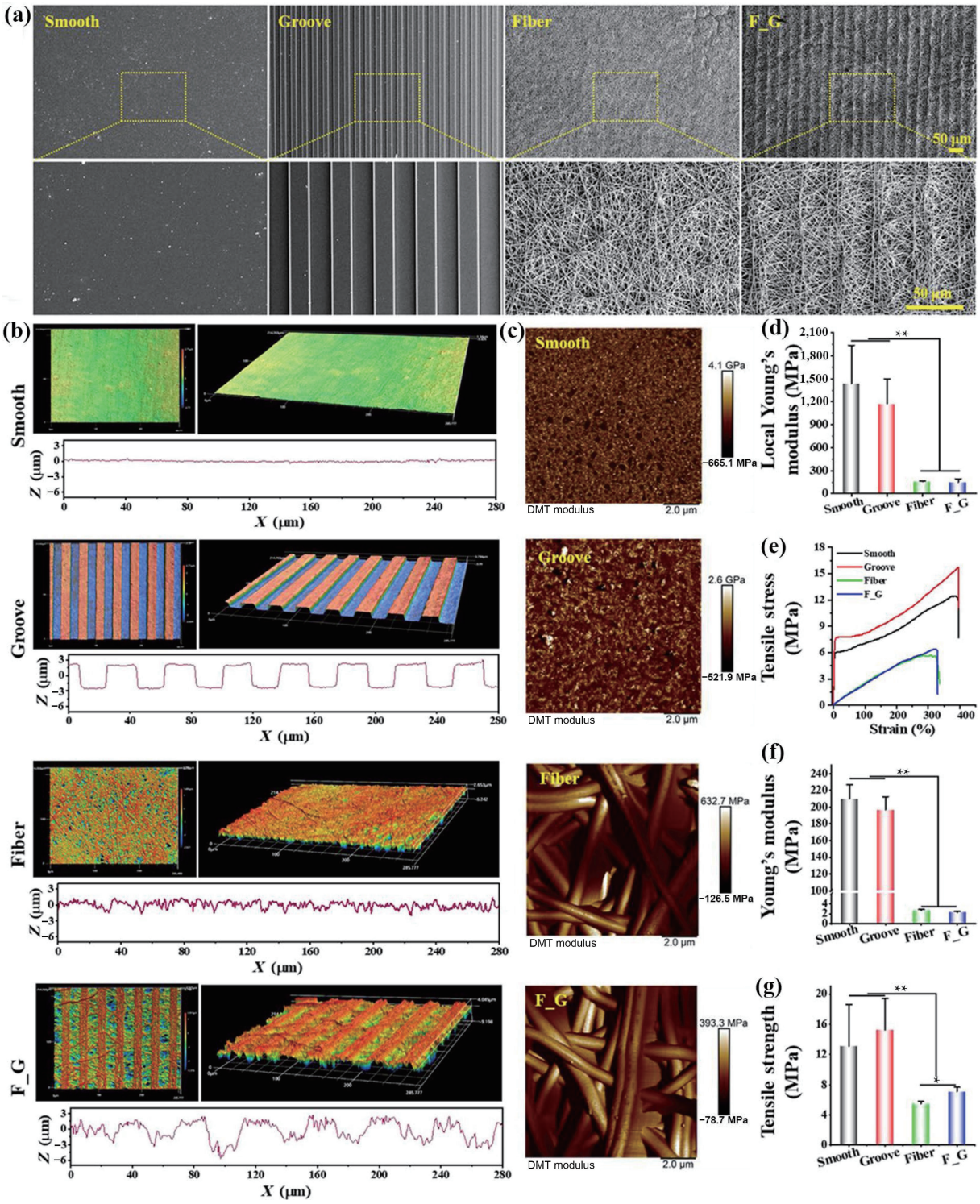

Figure 2 Characterizations of the obtained micropatterned nanofibrous membranes: (a) SEM images, (b) 3D surface topographies and cross-sectional linear scanning profiles, ((c) and (d)) AFM maps of modulus variations and averaged local Young's modulus, n = 3. (e)–(g) Bulk tensile properties including stress–strain curves, Young's modulus, and tensile strength, n = 8.

43.13 MPa. Similar to the AFM results, endowing the micropatterned film with ultrafine fibrous features also significantly reduced the bulk mechanical properties, such as Young's modulus reduced from 196.85 ± 15.36 to 2.27 ± 0.18 MPa, and tensile strength reduced from 15.25 ± 4.16 to 7.08 ± 0.61 MPa (Figs. 2(e) and 2(g)). The data confirmed the adequately lowered softness of the micropatterned nanofibers. Certainly, compared to smooth films, random nanofibers also exhibited an excellent softness with local modulus of 157.51 ± 4.95 MPa, bulk Young's modulus of 2.63 ± 0.23 MPa, and tensile strength of 5.47 ± 0.31 MPa. In brief, the micropatterned nanofibers present a distinct alternation of ridges and grooves (i.e., anisotropic topographic features), and adequate fiber softness.

3.2 Micropatterned nanofibers concurrently enhanced cell–cell and cell–matrix interactions to promote formation and maturation of endothelial monolayer

The nano-to-micron topological patterns of F_G significantly modulated the morphology and the actin polymerization of the regenerated HUVEC monolayer in a manner comparable to those of previous studies [29, 30]. As shown in Fig. 3(a), phalloidin

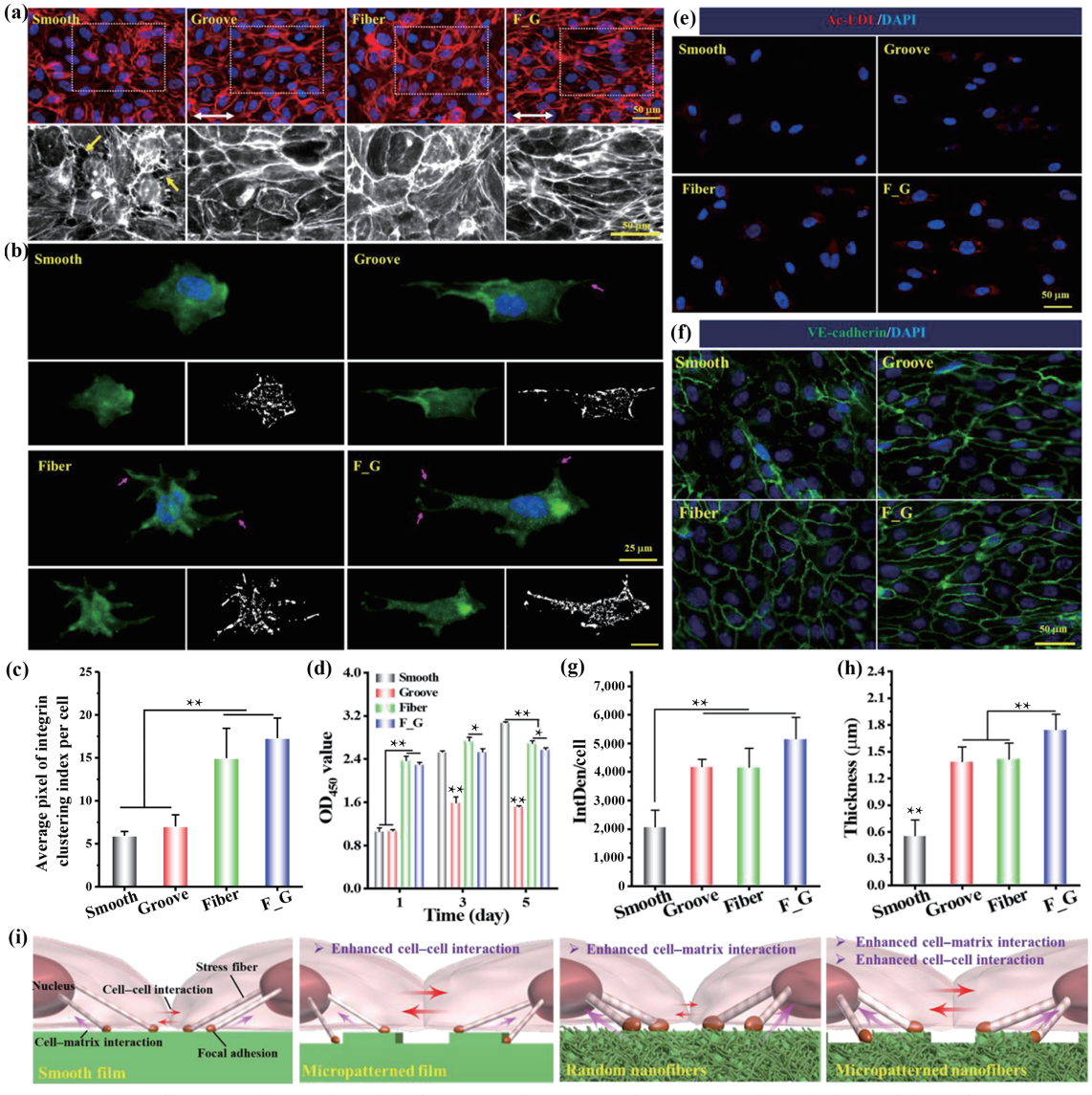

Figure 3 Micropatterned nanofibrous membranes enhanced the formation and maturation of HUVEC monolayer: (a) the cytoskeleton of HUVEC monolayer at day 3 of culture. The desaturated images (lower panel) are the local enlargement of immunofluorescence images. The white double-headed and yellow single-headed arrows indicate the microgroove direction and formed gaps between individual cells of the EC monolayer, respectively. (b) and (c) Immunofluorescence images of integrin β1 and the quantification of averaged size of FA sites per cell, integrin β1 (green), DAPI (blue), bar = 25 μm, n = 6. (d) Cell proliferation, n = 8. (e) and (f) Fluorescence images of Ac-LDL uptake (red), VE-cadherin (green), and nucleus (blue). (g) and (h) Quantified fluorescence intensity of Ac-LDL uptake from (e) and the thickness of cell–cell junctions from (f), n = 6. (i) Schematic of the micropatterned nanofibers-mediated the enhanced cell–matrix and cell–cell interactions for endothelial regeneration.

colocalized F-actin stress fibers were examined to analyze the collective actin organization in endothelial monolayer with fluorescence microscopy. Unlike the random morphology of HUVECs on Smooth and Fiber, the anisotropic microgrooves of both Groove and F_G led to a better cell elongation and preferential orientation of HUVECs, thus inducing the formation of a homogenous and confluent cell monolayer in anisotropic morphology. This supports the fact that the random nanofeatures on the surface of micropatterned nanofibers will not disrupt the contact guidance of parallel microgrooves to guide cell spreading and elongation. A further close look into the subtle cell-cell junctions revealed that although HUVECs were visually integrated with the neighboring cells for cell monolayer formation on all substrates, and cell–cell adhesive junctions with limited punctate contacts (yellow single-headed arrows) were noted between the adjacent cells on Smooth. That is, the slight gaps presented within the HUVEC monolayer were formed on smooth film, indicating the failure in forming a compact cell monolayer. In contrast, strong peripheral cortical arcs were observed around the cell–cell contacts in Groove group, which verified the excellent cell–cell interaction during endothelial regeneration *in vitro* [31]. Meanwhile, HUVECs displayed more neonatal and larger stress fibers assembled around the central region of the cell body on random nanofibers, manifesting the enhanced cell–substrate interactions for endothelial regeneration *in vitro* [12]. Furthermore, the confluent endothelial monolayer formed on F_G exhibited strong cortical arcs at cell–cell junctions with intensified stress fibers assembled in the cell body. This suggested that the micropatterned nanofibers could simultaneously enhance cell–cell and cell–matrix interactions for endothelial regeneration through synergistically utilizing the effects of microgroove patterns and nanofiber features.

With the noted softness, nanofibers may trigger the focal adhesion site dynamics of ECs to adapt the biomechanical cues of surrounding microenvironment, and then govern the cell–matrix interaction-triggered mechanotransduction pathways for hierarchical cellular control [21]. Thus, to verify the observed increase of cell–matrix interaction on the nanofibrous substrates,

the expression of integrin β1 in HUVECs was determined. Immunostaining images demonstrated the similar distribution of punctate FAs in the region of adherent cells on all substrates (Fig. 3(b)). However, from the averaged FA size per cell, larger-sized punctate FAs were found on nanofibrous substrates than those on the films, but no significant difference in the averaged FA size was observed between Smooth and Groove (or Fiber and F_G) (Fig. 3(c)). This indicated that nanoscale features seemed to alter FA dynamics more significantly than the microgroove features. The cell projected filopodia and lamellipodia also play a critical role in sensing a surface topography of localized microenvironment during contact guidance [32]. The apparent restriction on cellular lamellipodia spanning over the ridges of micropatterned samples indicated that 6 μm of groove depth was effective for aligning HUVECs. Furthermore, the increased amounts of filopodia exhibiting as thin extension of cellular membrane (pink single-headed arrows, Fig. 3(b)) on nanofibrous samples indicated that nanofiber patterns might be inclined to enhance the sensory ability of HUVECs for cell–matrix interaction.

In view of the noted enhancement of cell–cell and cell–matrix interactions, the micropatterned nanofibers were speculated to be capable of promoting the function and maturation of endothelial monolayer. Cell proliferation inside the HUVEC monolayer was examined first by CCK-8. The quantitative data revealed that the cell density increased by 191.31% for Smooth, 41.98% for Groove, 13.47% for Fiber, and 11.95% for F_G after 5 days of culture (Fig. 3(d)). Compared with smooth films, the lower growth rate of HUVECs when contacting the micropatterned films or random nanofibers implicated that both microgroove patterns and nanofibrous features could modulate the phenotype of confluent HUVECs to shift towards a quiescent state, and thus leading to the lowest cell growth rate on the micropatterned nanofibers. These findings signified that the dual-scaled topographic cues tended to provide a healthy microenvironment to prevent unwarranted cell expansion during endothelial remodeling. However, with regard to cell number at 1 day, nanofibers were recognized to support more cells adhering and growing than films. This attributes to their higher surface area for cellular interactions. To investigate the endothelial monolayer function, Ac-LDL uptake, a critical indicator of endocytosis ability, was examined (Figs. 3(e) and 3(g)). As shown, both microgroove patterns and nanofibrous features enhanced the Ac-LDL uptake of HUVECs, and the highest Ac-LDL uptake was found in F_G. Given the critical role of VE-cadherin-mediated adheren junctions in endothelial integrity and maturity [33], the state of cell–cell junctions inside the endothelial monolayer was further detected by VE-cadherin labeling. As shown in Fig. 3(f), the HUVEC monolayer on all samples exhibited obvious expression of VE-cadherin. However, VE-cadherin expressed at a higher level in the cells cultured on Groove and Fiber than that on Smooth, and the micropatterned nanofibers promoted the highest expression level of VE-cadherin (Fig. 3(h)). All data testified that the micropatterned nanofibers were able to promote the formation and maturation of native-like endothelial monolayer by concurrently enhancing cell–matrix and cell–cell interactions (Fig. 3(i)).

3.3 Microgroove patterns guided endothelial regeneration via enhanced expressions of integrin α5 and type I interleukin 1 receptor

The global transcriptomes of endothelial monolayer generated on Smooth and Groove were compared to reveal the underlying mechanisms involved in microgroove-mediated endothelial regeneration. Compared with Smooth, a total of 63 genes were differentially expressed in HUVECs cultured on Groove after 3 days of culture. Among them, 12 genes were significantly upregulated and 51 genes were downregulated (Fig. 4(a)). The detailed DEGs were shown in hierarchical clustering heatmaps (Fig. 4(b)). GO-term enrichment analysis was further performed to classify the genes with similar genetic functions in the biological process (Fig. 4(c)). Results demonstrated that the DEGs were correlated with cell cycle, cell division, chromosome segregation, regulation of inflammatory response, mitotic spindle assembly checkpoint and so on. With the classifications of upregulated and downregulated groups based on biological process (BP), cellular component (CC), and molecular function (MF), it was found that most of the top 15 terms belonged to the downregulated biological processes except for regulation of inflammatory response (Fig. 4(d)), indicating the leading roles of downregulated biological processes in microgroove-mediated endothelial remodeling.

Concretely, the upregulated DEGs involved in BP were enriched in the aspects of response to regulation of inflammatory response, response to interleukin-1 (IL-1), cell–cell adhesion via plasma membrane cell adhesion molecules, cell adhesion, obsolete negative regulation of LDL particle receptor biosynthetic process and so on (Fig. 4(d)). These BPs were noted to reflect the enhanced inflammatory regulation, cell–cell interaction, and endocytosis ability of endothelial monolayer. Concerning the top 2 terms of MF and CC enrichment, we found that the upregulated genes involved in MF were mainly enriched in response to protease binding and ECM protein binding while those involved in CC were closely correlated with clathrin-coated pit and integral component of plasma membrane. It has been recognized that clathrin-coated pits are the regions of the cell membrane specialized in receptor-mediated endocytosis [34]. These findings indicated that the parallel microgrooves could significantly enhance the endocytosis and alter the integral components of plasma membrane for protease binding and ECM protein binding, thereby resulting in the upregulated BPs. On the contrary, the enriched GO terms for the downregulated genes were mainly cell cycle, cell division, chromosome segregation, mitotic spindle assembly checkpoint, as well as microtubule bundle formation and so on. Most of the downregulated BPs were correlated to cell proliferation, supporting the enhanced quiescence state of endothelial monolayer on Groove. Since microtubules play a key role in forming the mitotic spindles that attach to chromosomes via kinetochores, and the anaphase-promoting complex are the major regulator of chromosome segregation [35, 36]. The significantly downregulated genes involved in the top 2 terms of MF and CC enrichment suggested that the parallel microgrooves were likely to downregulate cell proliferation through inhibiting microtubule binding and anaphase-promoting complex binding, thus suppressing chromosome segregation and mitosis.

To determine how the microgroove features exert their pro-endothelialization functions, KEGG pathway analysis was performed to gain insight into the potential mechanisms. The top 15 pathways of upregulated and downregulated KEGG enrichment are shown in Figs. 5(a) and 5(b), respectively. The significant upregulation of fluid shear stress and atherosclerosis reflected that parallel microgrooves took the role of stable blood flow laminar shear in guiding generation of native-like endothelium with oriented morphology, thus possessing remarkable effect of anti-atherogenesis [37]. The apparent downregulation of cell cycle in KEGG pathways verified the enlarged quiescence state of HUVEC monolayer induced by the microgroove patterns. Given that the upregulated BPs are closely associated with the alteration of integral components of plasma membrane (Fig. 4(d)), two essential components within cytomembrane of HUVECs, integrin α5 (ITGAV), and type I

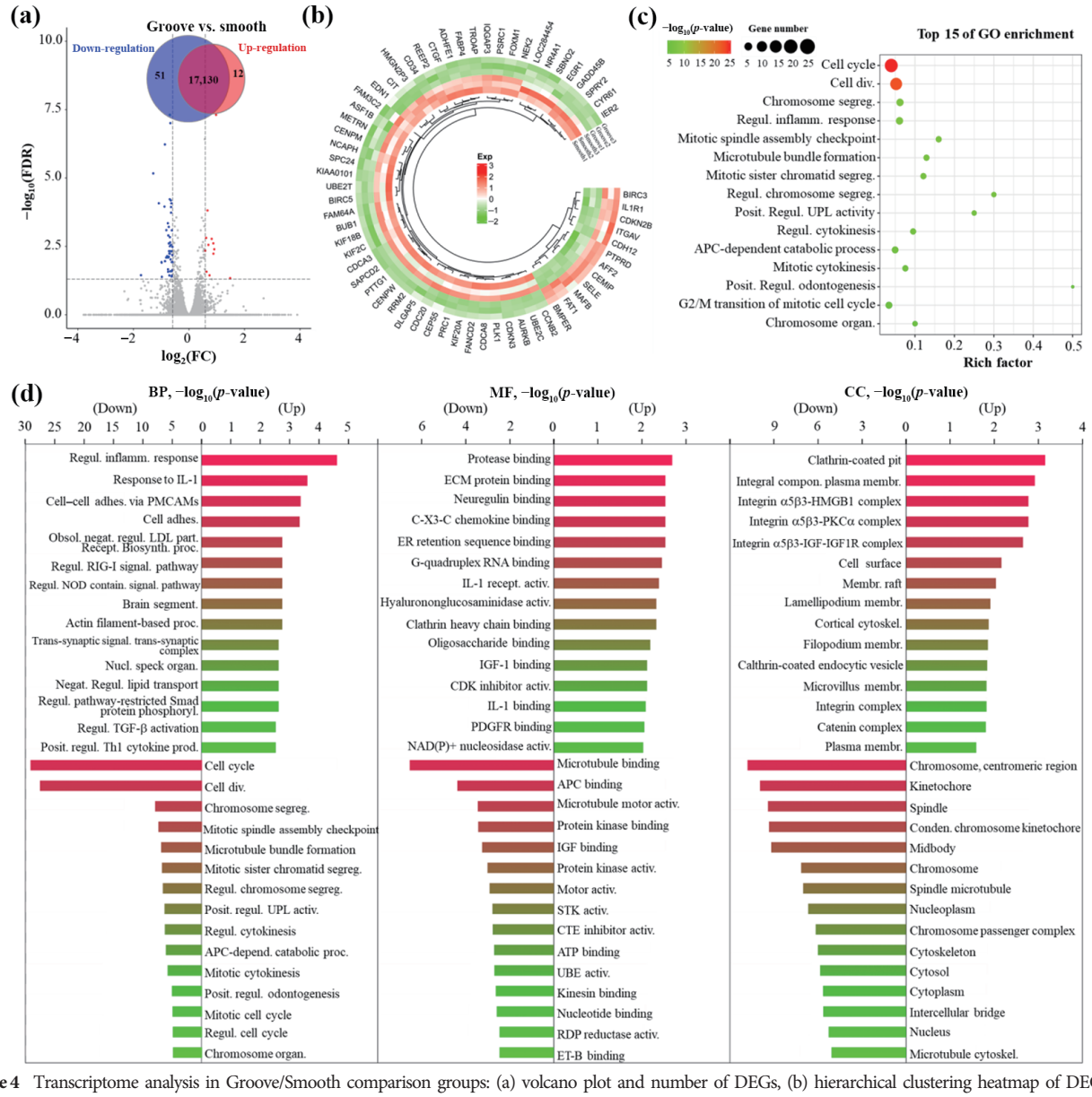

Figure 4 Transcriptome analysis in Groove/Smooth comparison groups: (a) volcano plot and number of DEGs, (b) hierarchical clustering heatmap of DEGs, (c) bubble chart of the top 15 significant GO terms, and (d) top 15 significant GO terms for the upregulated and downregulated DEGs in the categories of BP, CC, and MF. Full names of abbreviation see Table S1 in the ESM.

interleukin 1 receptor (IL1R1), were recognized from the 63 DEGs (Figs. 4(b) and 5(c)). Integrins have been demonstrated to play a pivotal role in cytoskeletal alignment under the stimulus of fluid shear stress [38], but enlargement of ITGAV-localised adhesion complex size is associated with microtubule network disruption [39]. The increased expression of ITGAV in fluid shear stress and atherosclerosis indicated that the microgroove features might disrupt microtubule assembly (as proven in downregulated MF in Fig. 4(d)) without affecting their ability to guide cell alignment via contact guidance, and thus to downregulate cell cycle of HUVECs. In the physiological and pathologic processes of ECs, IL-1 receptors are confirmed to regulate NF-kappa B signaling pathway [40] which has been found to directly suppress ubiquitin mediated proteolysis in this study (Fig. S3 in the ESM). However, ubiquitin proteolytic system plays an important role in a broad array of basic cellular processes including the regulation of cell cycle and modulation of the inflammatory responses [41]. Therefore, the enhanced IL1R1 expression indicated that the microgroove features were likely to modulate EC phenotype into quiescence state via IL1R1-mediated NF-kappa B signaling pathway followed by the downregulation of ubiquitin mediated proteolysis that suppresses cell cycle. In addition, cell cycle progression includes four phases: gap 1 (G1), DNA synthesis (S), gap 2 (G2), and mitosis (M) [42]. Depending on the DEGs enriched in cell cycle (Fig. 5(d) and Fig. S4 in the ESM), together with the downregulation of CycB that acts as a main factor influencing cell decision to enter mitosis [43], we could speculate that the microgroove features inhibited cell cycle by suppressing M-phase while activating G1-phase. In summary, in comparison to smooth surface, microgroove patterns were likely to promote endothelial remodeling via ITGAV-mediated microtubule disassembly, as well as IL1R1-activated NF-kappa B signaling pathways followed by the downregulation of ubiquitin mediated proteolysis, which further inhibits cell cycle of ECs through suppressing M-phase (Fig. 5(e)).

3.4 Nanofiber patterns guided endothelial regeneration via integrin α5β8-guided cell adhesion and MYLK/MYL9-mediated actin cytoskeleton remodeling

To reveal how random nanofibers affect endothelial regeneration, RNA-Seq was also performed to identify the transcriptional profile in HUVEC monolayer (Fiber vs. Smooth). After analyzing the

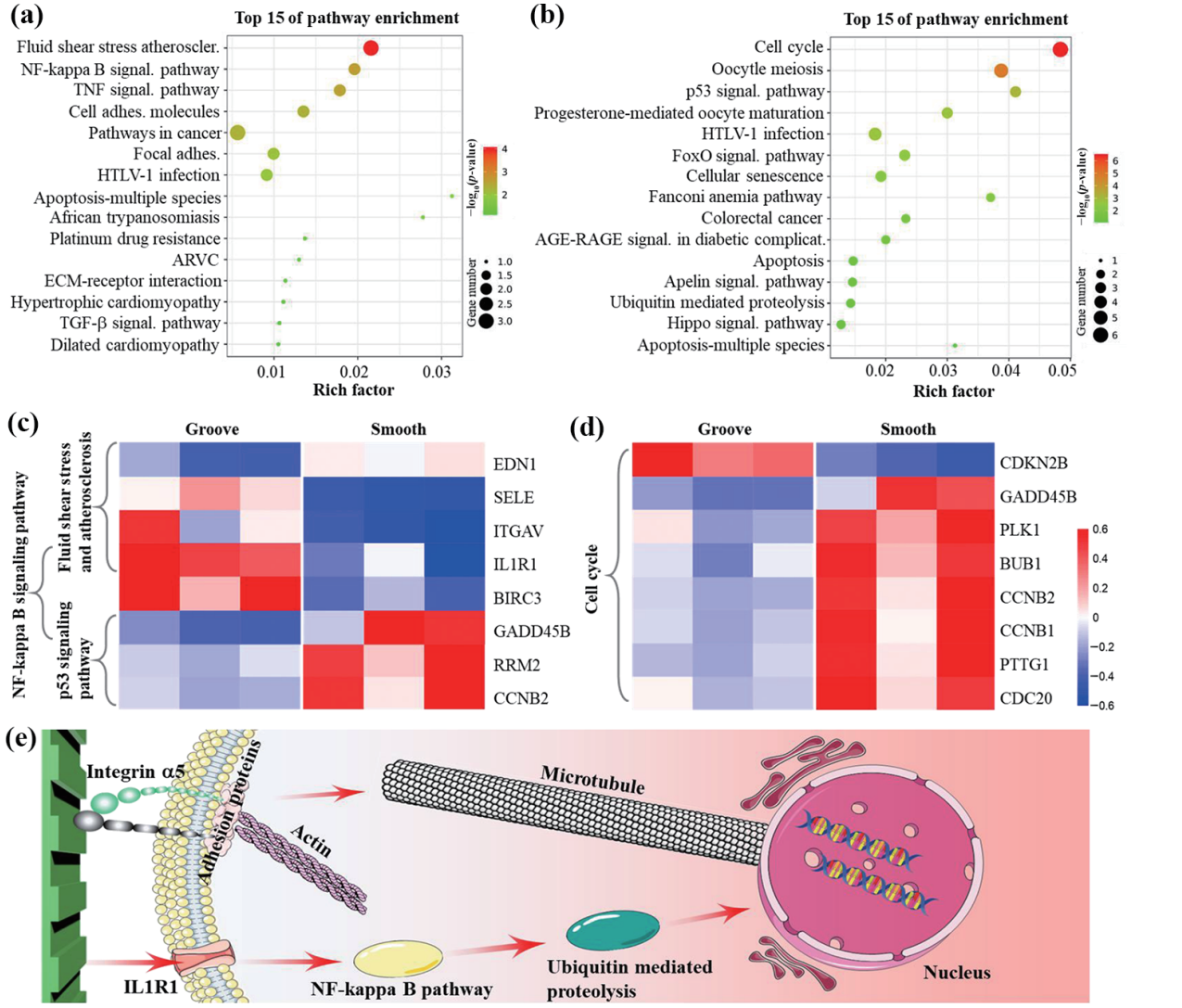

Figure 5 Mechanism analysis of parallel-microgroove-guided endothelial regeneration: ((a) and (b)) bubble chart of the top 15 significant KEGG pathways for the upregulated and downregulated DEGs; ((c) and (d)) heatmaps of the DEGs involved in fluid shear stress and atherosclerosis, NF-kappa B signaling pathway, p53 signaling pathway, and cell cycle; and (e) schematic representation of microgroove-pattern-guided signaling pathways in HUVECs. Full names of abbreviation see Table S1 in the ESM.

results with bioinformatics method, 527 genes were identified to be differentially expressed. Among them, 69 genes were upregulated and 458 genes were downregulated (Fig. 6(a)). The detailed DEGs were shown in hierarchical clustering heatmaps (Fig. 6(b)). Then, we performed GO enrichment analysis of these genes, and cluster analysis was used to explore the processes and function as shown in Fig. 6(c). The results indicated that nanofiber pattern-induced DEGs were closely related to cell cycle, cell division, chromosome segregation, mitotic spindle organization, mitotic sister chromatid segregation, and so on. Among the top 15 represented GO terms here, we found that most of DEGs were related to cell proliferation and vascular regeneration. After classifying them by upregulated and downregulated biological categories (Fig. 6(d)), we found that nanofiber patterns negatively regulated cell proliferation of HUVECs, which was similar to microgroove patterns.

Specifically, the results of BP suggested that the upregulated genes were enriched for those related to protein phosphorylation, regulation of transforming growth factor beta (TGF-β) activation, astrocyte cell migration, cell adhesion, cell adhesion mediated by integrin and so on (Fig. 6(d)). Through analyzing top 5 terms of MF and CC enrichment, we speculated that the random nanofibers might enhance cell–matrix interaction (ECM protein binding), induce cytoskeletal remodeling (myosin binding), and activate protein kinase via regulating integrins, collagen VI, and cytomembrane, resulting in the distinct upregulation of BPs in HUVECs. The enriched GO terms for the downregulated genes, such as cell cycle, cell division, chromosome segregation, and mitotic spindle organization, were found to be closely correlated with cell proliferation, which supports the results of CCK-8 (Fig. 3(d)). Furthermore, the significantly downregulated genes involved in the top 2 terms of MF and CC enrichment suggested that the suppression of cell proliferation induced by nanofiber patterns was mainly attributed to the inhibition of ECM binding and anaphase-promoting complex binding, which then affected chromosome segregation.

As for the underlying mechanisms, the results of upregulated KEGG pathways demonstrated that nanofiber patterns guided the cell behaviors of endothelial monolayer primarily through cytoskeleton-related mechanotransduction, such as focal adhesion and actin cytoskeleton regulation (Fig. 7(a)). Regulation of actin cytoskeleton has been demonstrated to be connected with the activation of protein phosphatases for signal transduction pathways [44], which is consistent with GO-analysis results (Fig. 6(d)). Attributing to the noted changes in actin cytoskeleton dynamics, fluid shear stress and atherosclerosis was also found to be significantly upregulated, because nanofiber patterns can act as the stimulation of stable blood flow laminar shear that promotes

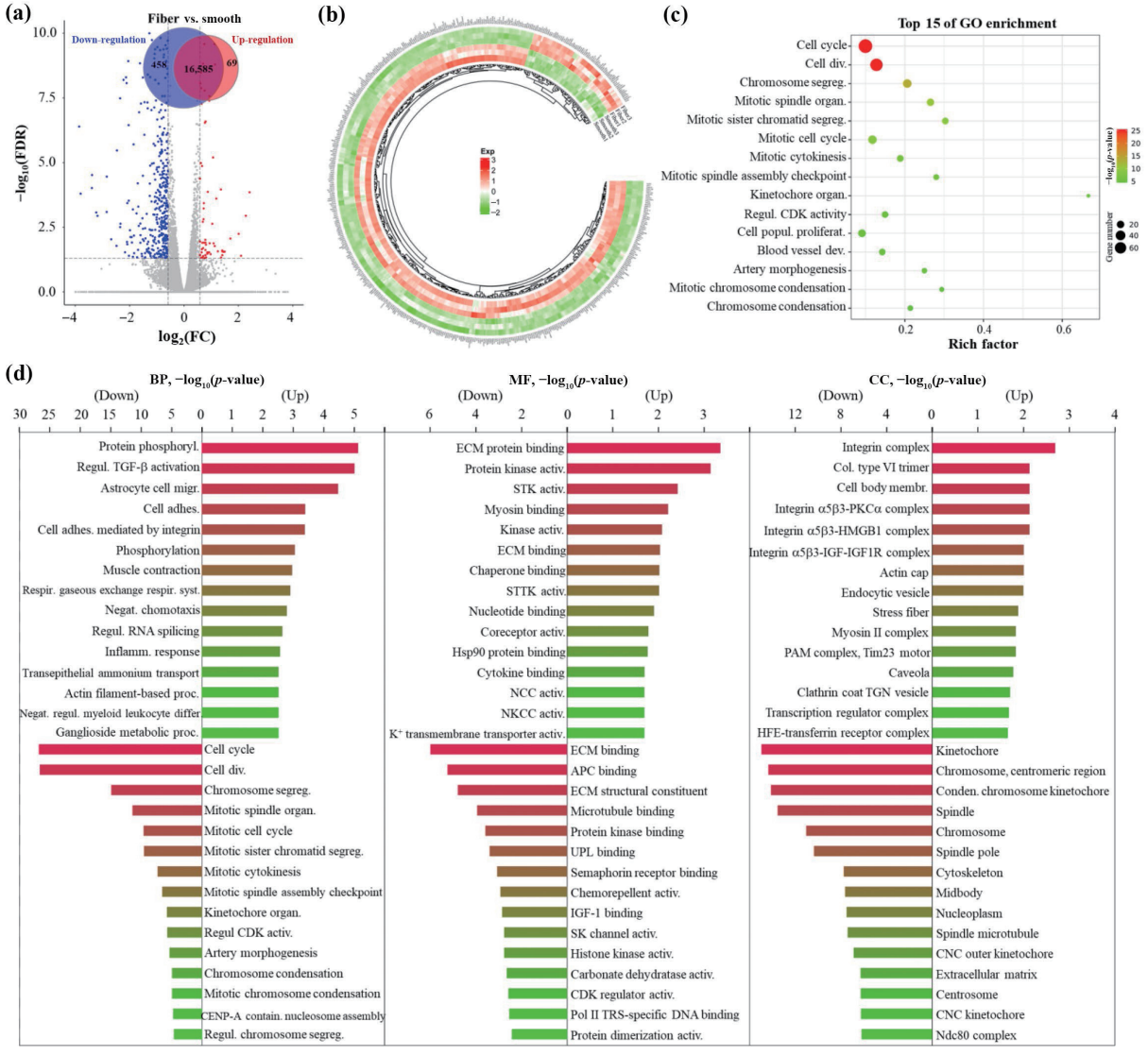

Figure 6 Transcriptome analysis in Fiber/Smooth comparison groups: (a) volcano plot and number of DEGs, (b) hierarchical clustering heatmap of DEGs, (c) bubble chart of the top 15 significant GO terms, and (d) top 15 significant GO terms for the upregulated and downregulated DEGs in the categories of BP, CC, and MF. Full names of abbreviation see Table S1 in the ESM.

the cytoskeleton remodeling via enhancing cell–matrix interaction, thereby suppressing the occurrence of atherogenesis [45, 46]. Meanwhile, the results of downregulated KEGG pathways showed that cell cycle was significantly downregulated by random nanofibers when compared with smooth films (Fig. 7(b)). That is, the quiescence state of the HUVEC monolayer was obviously enhanced by nanofiber patterns for endothelial maturity. From the involved DEGs, upregulation of ITGAV and integrin β8 (ITGB8) along with the downregulation of integrin β4 (ITGB4) were shown in focal adhesion (Fig. 7(c)). In the meantime, MYL9 BP and myosin light chain kinase (MYLK), related to myofibril assembly and stress fiber remodeling [47, 48], were markedly upregulated in the regulatory process of actin cytoskeleton. Together with the mechanotransduction process [17], these findings provided strong evidence that nanofiber patterns were involved in HUVEC behaviors by mediating integrin-managed focal adhesion followed by activating myosin light chain-mediated myofibril assembly. Furthermore, DIAPH3, localized at the centrosome during mitosis and regulating mitotic spindle assembly and bipolarity [49], was downregulated in the regulatory process of actin cytoskeleton, thus providing a good explanation for the noted suppression of cell cycle. Furthermore, the downregulated DEGs enriched in cell cycle inspired us to speculate that cell cycle was suppressed by random nanofibers via simultaneously suppressing G1, S, G2, and M-phases (Fig. 7(d) and Fig. S5 in the ESM). Additionally, ECM-receptor interaction was also found in the top 15 terms of downregulated KEGG pathways (Fig. 7(b)), in which the genes involved in ECM structural constituents, such as laminin α3 (LAMA3), type I collagen α2 (COL1A2), laminin β3 (LAMB3), and syndecan 1 (SDC1), were significantly downregulated (Fig. 7(e)). This may attribute to the biomimetic fineness and sufficient softness of random nanofibers that offer a suitable microenvironment, which favored ECs survival and growth in such a suitable niche [50]. Collectively, nanofiber patterns were likely to guide endothelial regeneration via integrin α5β8-guided cell adhesion and MYLK/MYL9-mediated actin cytoskeleton remodeling followed by DIAPH3-controlled cell cycle (Fig. 7(f)).

3.5 Endowing micropatterned film with soft nanofibers accelerated endothelial maturation via CXCR4/calcium-mediated actin cytoskeleton assembly

As shown in Fig. 3, a strategy of replacing the compact substrate that features parallel microgrooves with nanofibers, while retaining the microgroove surface patterns, was demonstrated to significantly enhance the ability of HUVECs to interact with the substrate, and then induced the formation of confluent and

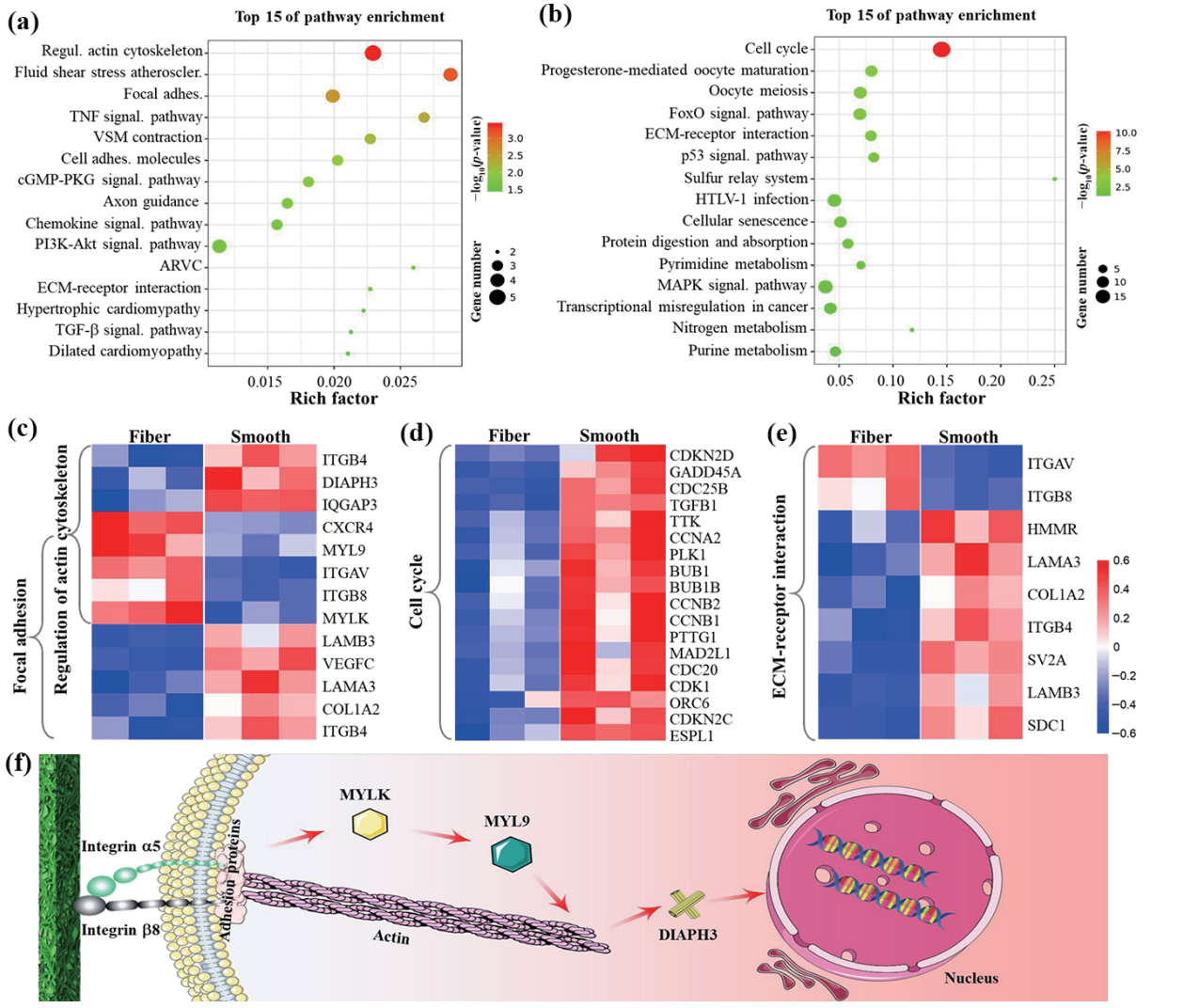

Figure 7 Mechanism analysis of random-nanofiber-guided endothelial regeneration: ((a) and (b)) bubble chart of the top 15 significant KEGG pathways for the upregulated and downregulated DEGs; ((c)–(e)) heatmaps of the DEGs involving actin cytoskeleton regulation, focal adhesion, cell cycle, and ECM-receptor interaction; and (f) Schematic representation of nanofiber-guided signaling pathways in HUVECs. Full names of abbreviation see Table S1 in the ESM.

oriented HUVEC monolayer with increased maturity. In order to confirm the findings, a gene expression profile of cells in F_G was performed. Compared to Groove, 254 genes were found to be differentially expressed, including 42 upregulated genes and 212 downregulated genes (Fig. 8(a)). Heatmap plot of these DEGs is shown in Fig. 8(b). After analyzing the genes with GO-term enrichment, we found that the DEGs fell into such different biological categories: ECM organization, response to hypoxia, negative regulation of fibroblast growth factor (FGF) receptor signaling pathway, cellular response to leptin stimulus, angiogenesis and so on (Fig. 8(c)). Similarly, most of these GO terms belong to the downregulated BPs (Fig. 8(d)).

In upregulated BPs, we found that in comparison to Groove, F_G affected HUVEC behaviors through upregulating the expression of genes that are related to mitochondrial adenosine triphosphate (ATP) synthesis coupled proton transport, ATP biosynthetic process, cristae formation, ATP metabolic process, regulation of cell adhesion and so on (Fig. 8(d)). As ATP is the critical energy carrier for cell metabolism [51], the upregulated genes involved in MF and CC indicated that in elongated and oriented endothelial monolayer, nanofiber-enhanced cell–matrix interaction showed excellent propensity to facilitate cell metabolism. On the contrary, in the downregulated BPs, the enriched GO terms were related to, but not limited to, ECM organization, negative regulation of FGF receptor signaling pathway, cellular response to leptin stimulus, and negative regulation of cell migration. Similar to random nanofibers, the biomimetic fineness and sufficient softness of micropatterned nanofibers offered a befitting microenvironment for cell growth, which resulted in the reduced expression of ECM structural constituents, especially for that conferring elasticity (the fourth term in MF). Due to the presence of microgroove patterns, integral component of plasma membrane was also found to be affected in F_G, but differently, it was downregulated compared to Groove. This indicated that the nanofiber patterns shown in F_G could effectively weaken the regulatory capacity of microgrooves in mediating cell membrane components.

Furthermore, KEGG pathway analysis was performed based on the DEGs in order to uncover the underlying signaling pathways that involve in F_G-regulated cell behaviors. The upregulated and downregulated pathways are shown in Figs. 9(a) and 9(b), respectively. Through scrutinizing these results, we found that F_G concurrently upregulated and downregulated several signaling pathways of HUVECs although the involvement levels might be different, such as leukocyte transendothelial migration and axon guidance. For example, leukocyte transendothelial migration was identified as the most upregulated signaling pathway, but only 2 genes including chemokine (C-X-C motif) receptor 4 (CXCR4) and myosin regulatory light chain 9 (MYL9) were positively involved in this pathway related DEGs (Fig. 9(c)).

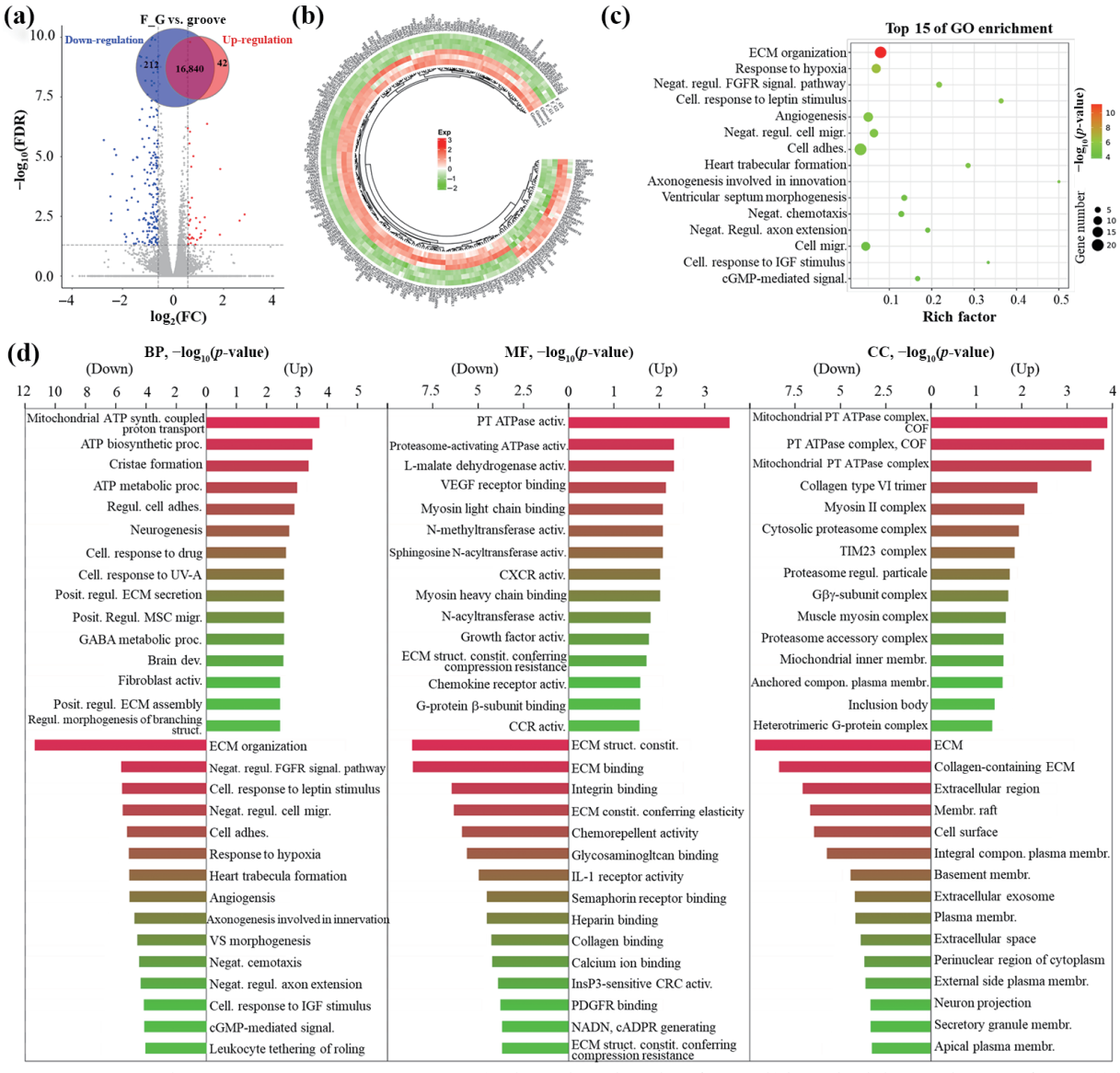

Figure 8 Transcriptome analysis in F_G/Groove comparison groups: (a) volcano plot and number of DEGs, (b) hierarchical clustering heatmap of DEGs, (c) bubble chart of the top 15 significant GO terms, and (d) top 15 significant GO terms for the upregulated and downregulated DEGs in the categories of BP, CC, and MF. Full names of abbreviation see Table S1 in the ESM.

Such a similar phenomenon also appeared in oxidative phosphorylation (Fig. S6 in the ESM) and axon guidance pathways (Fig. 9(c)). On the contrary, more genes were found to be downregulated in this pathway including integrin a4 (ITGA4), rap guanine nucleotide exchange factor 4 (RAPGEF4), junctional adhesion molecule 2 (JAM2), phospholipase C (PLC), gamma 2 (PLCG2), vascular cell adhesion molecule 1 (VCAM1), claudin 10 (CLDN10), and thy-1 cell surface antigen (THY1). Among them, ITGA4, JAM2, VCAM1, and THY1 have been demonstrated to play critical roles in mediating leukocyte adhesion on endothelium [52, 53]. The downregulation of these genes reflected that the enhanced ability of the regenerated HUVEC monolayer on F_G could inhibit leukocyte adhesion and leukocyte transendothelial migration as opposed to Groove. Axon guidance involves the sprouting, migration, and proliferation of ECs for angiogenesis [54]. Plenty of genes downregulated in this pathway indicated that under the guidance of parallel microgrooves, the attached nanofiber patterns tended to reduce the axon guidance of HUVECs, i.e., enhancing the quiescence state of endothelial monolayer. Additionally, advanced glycation end products-receptor for advanced glycation end products (AGE-RAGE) signaling pathway has been highlighted to promote diabetes-mediated vascular calcification by increasing collagen deposition for tissue fibrosis [55]. Meanwhile, disturbed blood flow, i.e., low or oscillatory shear stress, has also been recognized as a critical cue to exacerbate vascular dysfunction, such as promoting expression of VCAM1 and PRKCZ (protein kinase C, zeta) to induce atherosclerosis [56]. Hence, the significant downregulation of these two pathways (Fig. 9(d)) suggested that the nanofiber-featured microgrooves were more beneficial for enhancing endothelial function and reducing the occurrence of vascular complications, compared to compact film-featured microgrooves, which was further verified by the downregulation of platelet activation, a key process for thrombosis (Fig. 9(b)).

Furthermore, CXCR4, serving as a chemokine receptor that sits in the cytomembrane of ECs and can be directly affected by cell–matrix interaction [57], was also found to be upregulated by F_G in this study. Thus, a simplest view of the underlying signaling pathway was speculated to begin with the chemokine signaling pathway. Interestingly, it is well-recognized that chemokine receptors can stimulate the response of phospholipase C and then elicit calcium mobilization [58, 59]. Such a signaling pathway line was also speculated to be suitable for F_G-mediated cell behaviors, with the evidences of the downregulated PLCG2, as

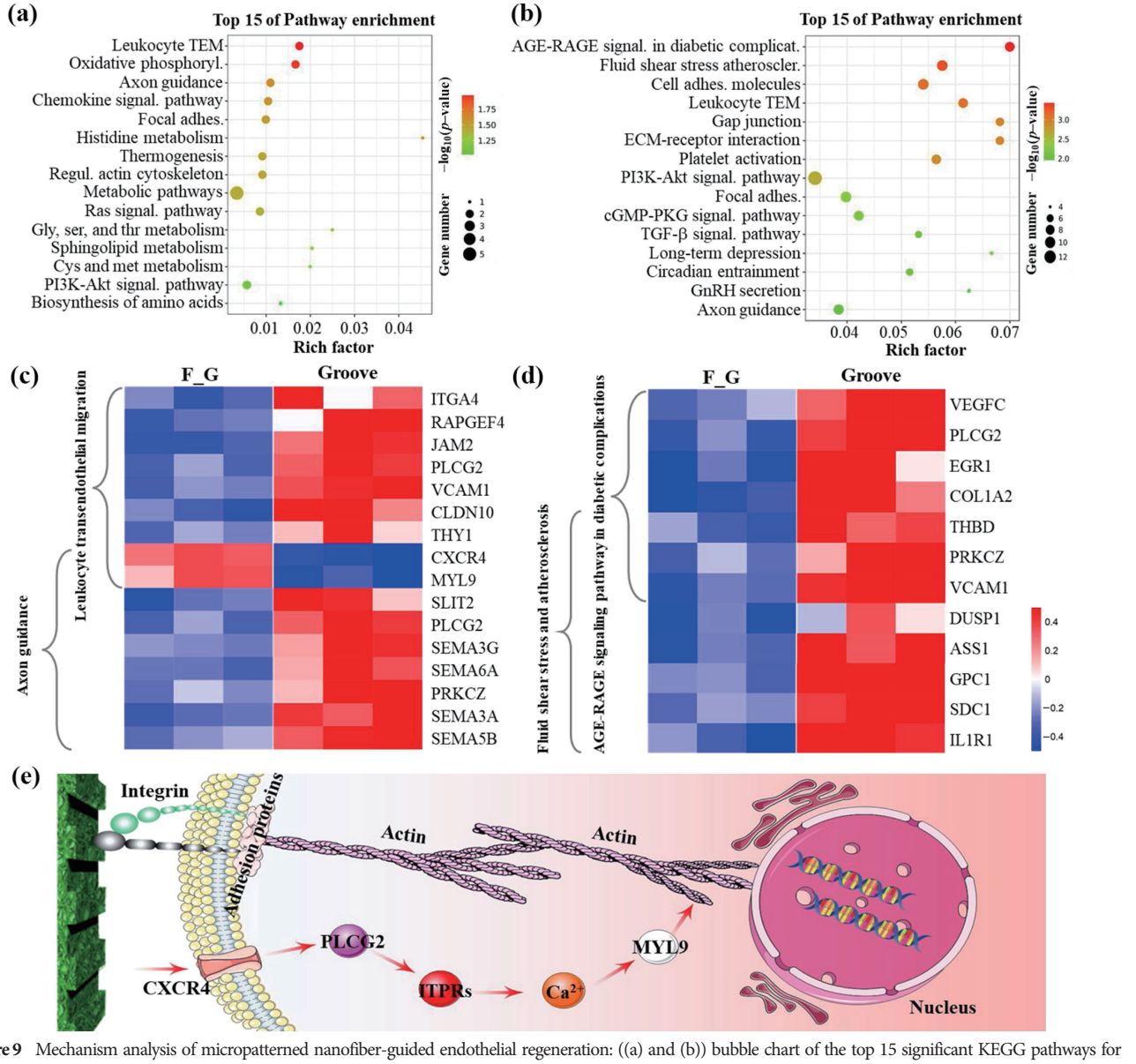

Figure 9 Mechanism analysis of micropatterned nanofiber-guided endothelial regeneration: ((a) and (b)) bubble chart of the top 15 significant KEGG pathways for the upregulated and downregulated DEGs; ((c) and (d)) heatmaps of the DEGs involving leukocyte transendothelial migration, axon guidance, AGE-RAGE signaling pathway in diabetic complications, and fluid shear stress and atherosclerosis; and (e) schematic representation of micropatterned nanofiber-guided signaling pathways in HUVECs. Full names of abbreviation see Table S1 in the ESM.

well as the downregulated type-I and type-II inositol 1,4,5-trisphosphate receptor (ITPR) that play a critical role in mediating calcium signaling pathway [60]. Furthermore, ITPR-induced Ca^{2+} waves have been demonstrated to be closely associated with ATP-mediated microfilament and microtubule assembly [60]. Thus, the significantly enhanced expression of MYL9 (Fig. 9(c)) and the upregulated ATP-related BPs (Fig. 8(d)) suggested that under the guidance of parallel microgrooves, the attached nanofiber patterns are likely to modulate HUVEC behaviors via CXCR4/calcium-mediated actin cytoskeleton assembly (Fig. 9(e)).

3.6 Numerical simulation confirmed the potential stable hemodynamics on the micropatterned nanofiber surface

Hemodynamics is likely to be affected by the surface topological patterns of TEVGs for thrombogenesis [61, 62]. Given an effective method to analyze the effect of substrate geometry on the blood flow features [63], numerical simulation was further explored to assess the potential value of the micropatterned nanofibers for constructing TEVGs. A numerical model of hemodynamics was built according to surface SEM images of substrates (Fig. 10(a)). As shown, the inner surface topography can significantly influence blood flow velocity and hemodynamics. The 3D streamline and surface streamline clearly confirmed that featuring substrate with parallel microgrooves availed to reduce blood retention (pink single-headed arrows) on substrate surface and brought in more uniform distribution of blood flow when compared to that of non-oriented grafts (Fig. 10(b)). Because of the copresence of microgroove and nanofiber patterns, the slightest blood retention was observed on F_G surface. Besides, when the blood flow meets obstacles, hemodynamics will be destructive and a sudden decrease of blood flow velocity will occur, as proven in Fiber. Interestingly, the appearance of parallel microgrooves along the direction of blood flow obviously inhibited the severe turbulence caused by fiber intersections (Fig. 10(c)). Collectively, our findings indicate that in the micropatterned nanofibers, although their nanofibrous architecture exhibits the risk of perturbing hemodynamics, their parallel microgroove surface demonstrates a positive impact on maintaining stable blood flow velocity and hemodynamics, which is consistent with the previous study [61], thereby supporting its applicational prospects in constructing TEVGs.

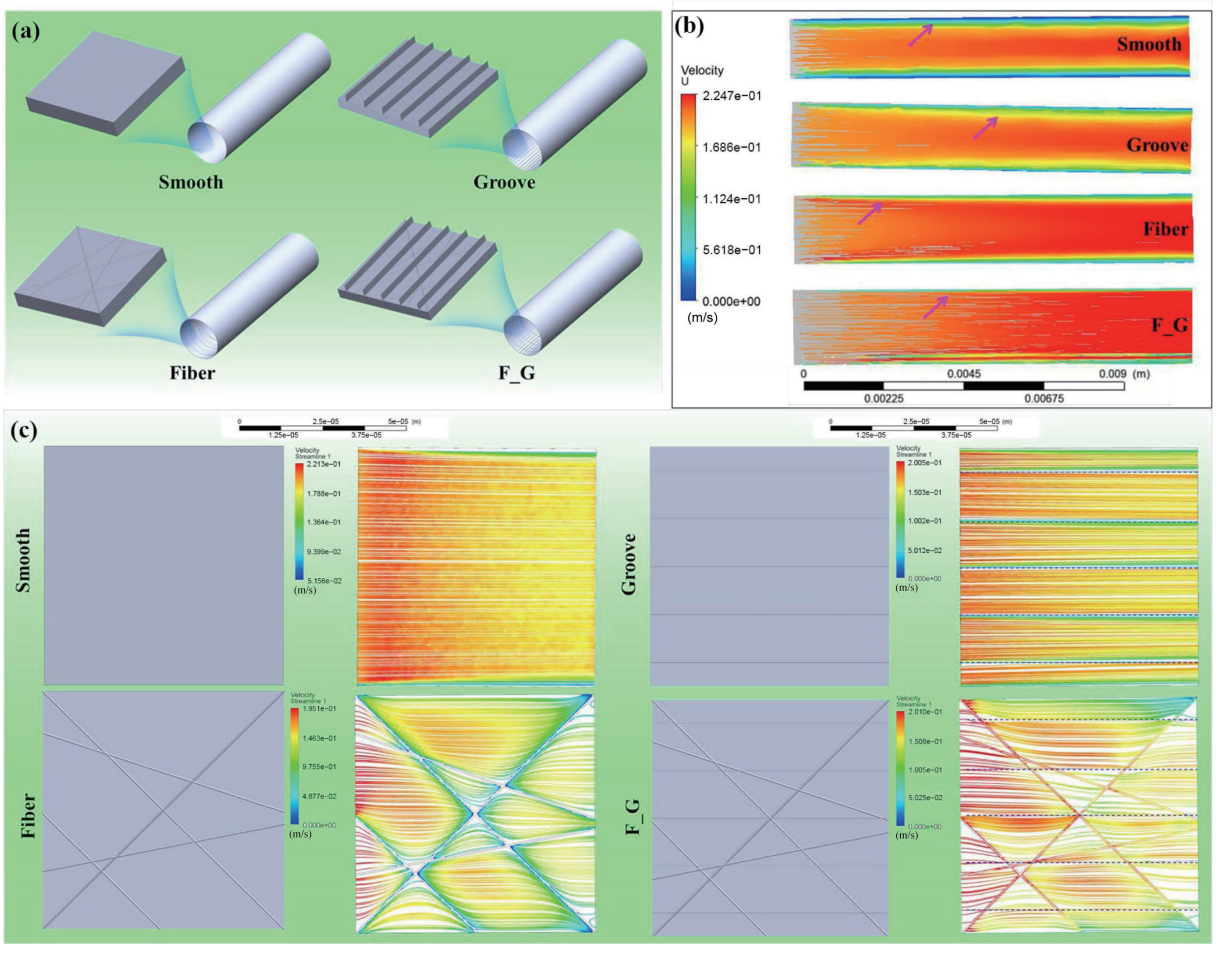

Figure 10 Numerical simulation of blood flow velocity on the micropatterned nanofibrous membranes: (a) simulation model, (b) 3D streamline, and (c) surface streamline.

4 Discussion

In terms of vascular grafts, regenerating a healthy endothelium on the inner surface of TEVGs is extremely desirable for preventing undesired post-implantation complications. As growing evidences demonstrate that the complete formation of an EC monolayer is not synonymous with the restoration of healthy endothelial function. How to improve the endothelial functions of the regenerated endothelium has been recognized as a vital determinant for TEVG-guided vascular regeneration and remodeling *in vivo*, although it remains a great challenge thus far. Over the past few decades, plenty of efforts have been made to provide insights into the topographic modification of the substrate with parallel microgrooves, and thus to regenerate native-like aligned endothelium [16, 32]. It has also been demonstrated that such structural patterns could effectively induce cell alignment via lamellipodia-driven contact guidance [16]. Certainly, the function of the regenerated endothelium is also significantly improved by the surface microgrooves, such as enhancing cell-to-cell junctions [23], reducing leukocyte transendothelial migration [64], and inducing an athero-resistant phenotype [4], as verified in this work (Fig. 3). Nevertheless, from the aspect of mechanics-dependent communication in cell–matrix interaction, the current-used substrates featuring microgroove patterns are commonly correlated with an unbefitting high stiffness that makes cells hardly to remodel the microenvironment to achieve their requirements [21], which impede healthy endothelium remodeling under the action of a persistent force-feedback loop between matrix and cells. Because of the ability to precisely control the stiffness, elastic hydrogels have been widely used to investigate how cells sense stiffness, and demonstrated that the hydrogel stiffness sensed by cells is in the pascal to kilopascal range [65]. Different from the hydrogel materials, nanofibrous system recapitulates the fibrous meshwork of natural ECM, thus providing an appropriate topographical cue for cell–matrix interaction [66]. Due to their special mechanical behavior and the high independence of each fiber, nanofibrous substrates allow cells to remodel them at high stiffness (~ 140 MPa of modulus), which is about several orders of magnitude higher than that of hydrogels (less than 30 kPa) [22, 66]. This indicated that the nanofibers with the ~ 149 MPa modulus in this study are feasible for cells to remodel them and adapt the microenvironment. As proven in this work, in comparison to smooth film, random nanofibers were found to trigger the FA site dynamics of ECs and promote the formation of compact endothelial monolayer through enhanced cell–matrix interactions (Fig. 3(b)). However, traditional viewpoint suggests that high substrate stiffness was deemed to increase cell–substrate interaction in view of the increased assembly of actin filaments [17]. This is because, to balance the intra and extracellular forces, cytoskeleton assembly is facilitated to bear high traction force in stiff environment [21]. Although the enhanced cytoskeleton assembly is usually synonymous with the increased ability of cells to manipulate matrix, once substrate stiffening is over a certain threshold, such induced cellular responses will lead to the difficulty for cells to remodel and adapt the substrate. This explains that substrate stiffness has been demonstrated to be negatively correlated with the integrity and function of EC monolayer [1, 2], in which stiffer substrate exacerbated the disruptive effects on intercellular force transduction signals within EC monolayer by increasing heterogeneity in stress distributions [33]. Therefore, cell–matrix interaction is not as simple as the traditional opinion

that stiff environment enhances cells' ability to interact with their matrices, at least in EC function case.

Accumulating evidences demonstrate that parallel microgrooves can induce the formation of an oriented endothelium and nanofibers can increase the cell–matrix interaction for endothelium maturity. Based on the aforementioned findings, we speculate that replacing the micropatterned substrate with a nanofibrous micropatterned substrate may provide a promising strategy to realize successful engineering of a healthy endothelium. As a biodegradable elastic synthetic polymer that has been widely used for constructing TEVGs [12, 26], PLCL was chosen to be electrospun into nanofibers. It is obvious that combining electrospinning and soft lithography technique can successfully realize the topographic modification of random PLCL nanofibers with the parallel microgroove patterns (Fig. 2). Attributing to its simpleness, convenience, and effectiveness, the strategy was speculated to be capable of generating high-resolution microgrooves on various substrates. After that, the obtained micropatterned nanofibers were also demonstrated not only able to effectively guide cell elongation and orientation to form a confluent cell monolayer with anisotropic morphology, but also able to significantly enhance the maturation of the regenerated endothelium via promoting cell–cell and cell–fiber interactions (Fig. 3). In general, cell–cell interaction is positively associated with endothelium maturity. Previous studies have confirmed that increasing topographical variation could inhibit endothelium maturity and disrupt endothelial cell–cell junction organization via increasing cytoskeletal contractility, which in turn induces EC proliferation, EC monolayer disruption, and neutrophil transmigration [11, 31, 33]. Therefore, the successful formation of oriented HUVEC monolayer induced by parallel microgrooves indicates that ~ 5 μm of groove depth will be an effective topographic cue to guide HUVEC orientation and to avoid the disruption of cell–cell junction. Additionally, after implantation *in vivo*, the increased cell–matrix interaction will effectively prevent the detachment of EC monolayer from TEVG surface likely caused by fluid shear stress when micropatterned nanofibers are employed as a particular topographical surface.

Previously, specific topographic cues that simulate the feature dimensions and types of ECM could influence an array of fundamental EC behaviors [67]. However, the mechanism or the genes responsible for this wide variability of cell behaviors remain poorly understood. Hence, transcriptome analysis was performed in this work to understand how different biomimetic scales (e.g., parallel microgrooves, nanofibers, and micropatterned nanofibers) influence cell behavior and gene expression, which greatly aided the intelligent design of vascular grafts (Figs. 4–9). The number of DEGs (527 genes) in Fiber/Smooth comparison group was much more than that (63 genes) in Groove/Smooth comparison group, suggesting that the effect of nanofibrous patterns on HUVEC behaviors is more noticeable than that of microgroove patterns. However, in F_G/Groove comparison group, the micropatterned nanofibers induced less gene expression changes (254 genes) than nanofibers in Fiber/Smooth comparison group, indicating that the presence of microgroove cue might weaken the regulatory ability of nanofibers on HUVEC behaviors. Furthermore, parallel microgrooves were able to guide endothelial regeneration via regulating several components of cytomembrane during contact guidance, such as ITGAV and IL1R1 (Figs. 4 and 5). Differently, nanofiber patterns were demonstrated to guide endothelial regeneration via regulating focal adhesion and actin cytoskeleton remodeling (Figs. 6 and 7). As well known, the actin cytoskeleton is a dynamic structure that organizes cell membrane and guides cellular physiology associated with the membrane such as ion channels and transporters [68]. When cells adhere on a substrate, the substrate surface topographic cues will activate intracellular signals in several ways: a) activating specific actin binding proteins to regulate actin polymerization dynamics, b) activating phosphatases or protein kinases to regulate phosphorylation of specific cytoskeletal proteins, and c) activating signal transduction pathways from membrane receptor activation to cytoskeleton reorganization [44]. These findings are in agreement of our finding that micropatterned nanofibers can accelerate endothelial maturation via CXCR4/calcium-mediated actin cytoskeleton assembly in which ATP-mediated biological processes are involved (Fig. 9). Moreover, when ECs reach an equilibrium and stabilize their phenotype, ECM products will be reduced in regenerated endothelium [50]. In support of this, a significant decrease in ECM organization was observed when HUVECs were exposed to random nanofibrous or micropatterned nanofibrous patterns (Figs. 7 and 8), indicating that the substrates offer a suitable microenvironment for healthy endothelial remodeling.

Additionally, in TEVG-mediated vascular regeneration, disruption of vascular homeostasis has also been recognized as one of the principal mechanisms in causing undesired complications and occlusion-resultant failure. The fluid shear force generated by blood flow has a crucial influence on the thrombus formation and modulation of blood cell behaviors [69], which already has been used as an indicative marker to monitor the patency of artificial vessels [61]. Therefore, as one of the representative blood-contacting implants, TEVGs are also required to be rationally designed with surface topography modification to maintain stable vascular homeostasis. Interestingly, in this study we confirmed that although the increased obstacles on nanofiber membrane surface had certain risks in destructing hemodynamics in comparison to smooth film, it significantly reduced blood retention on substrate surface. Furthermore, featuring the membrane with parallel microgrooves was demonstrated able to effectively inhibit the severe turbulence and regain even blood flow (Fig. 10). Besides, from the perspective of clinic application, even though micropatterned films showed excellent propensity to promote oriented endothelial formation and enhance even blood flow, their compact architecture displayed fatal drawbacks in inhibiting cell infiltration and nutrition diffusion, thus inhibiting matrix remodeling and vascular regeneration. *In vivo*, altered hemodynamics also plays a causative role in endothelial dysfunction [70]. It is definite that the stable laminar flow induces elongation of endothelial cells and activates ECs to inhibit coagulation and resists the inflammatory response [71]. In contrast, the disturbed/oscillatory flow leads to the cobblestone-like morphology of ECs, thus destroying the integrity of endothelial monolayer, increasing oxygen stress, and inducing endothelial cell aging [72]. This indicates that the increased stability of fluid flow on the micropatterned nanofibrous substrates is capable of promoting the healthy remodeling of native-like endothelium compared to that on random nanofibers. All findings support the applicational prospects of micropatterned nanofibers in constructing TEVGs. Additionally, surface nanotopography has a crucial influence on thrombosis through a cascade of biological processes, such as plasma protein adsorption, blood platelet adhesion and activation, and clot stabilization [12]. Parallel microgroove patterns was proven to have excellent propensity to inhibit platelet activation (Fig. S7 in the ESM), which is consistent with previous study [61]. In addition, increased platelet activation by nanofiber patterns indicates that constructing TEVGs simply via surface topography modification can hardly satisfy all the clinical needs for healthy vascular regeneration. In this case, further modifications are necessary, such as grafting bioactive molecules, accurate control of stiffness, and creating a

self-adaptive microenvironment for cells.

Summarily, the main objective of this study was to topologically modify the micropatterned substrate with soft PLCL nanofibers in order to enhance both cell–cell and cell–matrix interactions, thus promoting the formation and maturity of regenerated endothelium. While the goal was generally achieved and results demonstrated that the enhanced endothelial remodeling was likely ascribed to the signaling pathway of CXCR4/calcium-mediated actin cytoskeleton assembly, the study still has several limitations which are worthy of further verification in the future. Firstly, this study was performed based on a definite surface topography (groove width: ~ 15 μm; groove depth: ~ 5 μm; nanofiber diameter: ~ 0.5 μm), given the complexity involved in the influence of surface topography on HUVEC behaviors, further research should be performed to provide more evidences for the optimal structuring within the micropatterned nanofibrous topography. Secondly, although both microgrooves and nanofibers enable ECs to improve endothelial regeneration, whether such surface structures will exert side-effects remains unclear. For instance, will the upregulated expression of IL-1R found in microgroove-guided HUVECs activate inflammatory cells? Does the decreased expression of ECM-related proteins found in nanofiber-guided HUVECs inhibit matrix remodeling during vascular regeneration? Furthermore, the mechanistic investigation explored by transcriptome analysis is limited, additional experiments are warranted to verify the preliminarily explored mechanism. Lastly, the role and process of such micropatterned nanofibrous scaffolds in guiding healthy endothelial remodeling should be further observed and verified *in vivo*. Even with these limitations, our results still support an affirmation that the micropatterned nanofibers can provide an innovative method for constructing TEVGs that are able to promote regeneration and maturation of native-like endothelium.

5 Conclusions

We have successfully modified the micropatterned substrate topologically with soft PLCL nanofibers to obtain a micropatterned nanofibrous scaffold, and demonstrated that such modification not only retained the surface high-resolution parallel microgrooves (~ 5 μm of groove depth), but also attached an adequate softness to the substrate. To one's surprise, the micropatterned nanofibers were verified to significantly promote the regeneration and maturation of native-like endothelium through synchronously increasing cell–cell and cell–matrix interactions. As parallel microgrooves guide endothelial regeneration via regulating cytomembrane components whereas nanofiber patterns guide endothelial regeneration via modulating actin cytoskeleton remodeling, the micropatterned nanofibers were demonstrated to accelerate endothelial maturation via CXCR4/calcium-mediated actin cytoskeleton assembly. Lastly, a positive impact of the micropatterned nanofibers on maintaining stable hemodynamics further supported their applicational prospects in constructing TEVGs.

Acknowledgements

This work was supported by National Key Research and Development Program of China (No. 2018YFC1105800), China Postdoctoral Science Foundation (No. 2020M681322), and National Natural Science Foundation of China (No. 31870967). We are also grateful to Shiyanjia Lab (www.shiyanjia.com) for his kind help in performing the numerical simulations.

Electronic Supplementary Material: Supplementary material (detailed methods of transcriptome analysis, full name of abbreviations in transcriptome analysis, further details of the substrate formation and topography analysis, additional information for transcriptome sequencing and platelet activation) is available in the online version of this article at https://doi.org/10.1007/s12274-022-4670-2.

References

[1] Urbano, R. L.; Furia, C.; Basehore, S.; Clyne, A. M. Stiff substrates increase inflammation-induced endothelial monolayer tension and permeability. *Biophys. J.* **2017**, *113*, 645–655.

[2] Yi, B. C.; Shen, Y. B.; Tang, H.; Wang, X. L.; Zhang, Y. Z. Stiffness of the aligned fibers affects structural and functional integrity of the oriented endothelial cells. *Acta Biomater.* **2020**, *108*, 237–249.

[3] Bonito, V.; Koch, S. E.; Krebber, M. M.; Carvajal-Berrio, D. A.; Marzi, J.; Duijvelshoff, R.; Lurier, E. B.; Buscone, S.; Dekker, S.; De Jong, S. M. J. et al. Distinct effects of heparin and interleukin-4 functionalization on macrophage polarization and *in situ* arterial tissue regeneration using resorbable supramolecular vascular grafts in rats. *Adv. Healthc. Mater.* **2021**, *10*, 2101103.

[4] Gupta, P.; Mandal, B. B. Silk biomaterials for vascular tissue engineering applications. *Acta Biomater.* **2021**, *134*, 79–106.

[5] Koch, S. E.; De Kort, B. J.; Holshuijsen, N.; Brouwer, H. F. M.; Van Der Valk, D. C.; Dankers, P. Y. W.; Van Luijk, J. A. K. R.; Hooijmans, C. R.; De Vries, R. B. M.; Bouten, C. V. C. et al. Animal studies for the evaluation of *in situ* tissue-engineered vascular grafts—A systematic review, evidence map, and meta-analysis. *Npj Regen. Med.* **2022**, *7*, 17.

[6] Radke, D.; Jia, W. K.; Sharma, D.; Fena, K.; Wang, G. F.; Goldman, J.; Zhao, F. Tissue engineering at the blood-contacting surface: A review of challenges and strategies in vascular graft development. *Adv. Healthc. Mater.* **2018**, *7*, 1701461.

[7] Hao, D. K.; Fan, Y. H.; Xiao, W. W.; Liu, R. W.; Pivetti, C.; Walimbe, T.; Guo, F. Z.; Zhang, X. K.; Farmer, D. L.; Wang, F. S. et al. Rapid endothelialization of small diameter vascular grafts by a bioactive integrin-binding ligand specifically targeting endothelial progenitor cells and endothelial cells. *Acta Biomater.* **2020**, *108*, 178–193.

[8] Peng, B.; Tong, Z. Q.; Tong, W. Y.; Pasic, P. J.; Oddo, A.; Dai, Y. T.; Luo, M. H.; Frescene, J.; Welch, N. G.; Easton, C. D. et al. *In situ* surface modification of microfluidic blood-brain-barriers for improved screening of small molecules and nanoparticles. *ACS Appl. Mater. Interfaces* **2020**, *12*, 56753–56766.

[9] Zhuang, Y.; Zhang, C. L.; Cheng, M. J.; Huang, J. Y.; Liu, Q. C.; Yuan, G. Y.; Lin, K. L.; Yu, H. B. Challenges and strategies for *in situ* endothelialization and long-term lumen patency of vascular grafts. *Bioact. Mater.* **2021**, *6*, 1791–1809.

[10] Chang, H.; Hu, M.; Zhang, H.; Ren, K. F.; Li, B. C.; Li, H.; Wang, L. M.; Lei, W. X.; Ji, J. Improved endothelial function of endothelial cell monolayer on the soft polyelectrolyte multilayer film with matrix-bound vascular endothelial growth factor. *ACS Appl. Mater. Interfaces* **2016**, *8*, 14357–14366.

[11] Krishnan, R.; Klumpers, D. D.; Park, C. Y.; Rajendran, K.; Trepat, X.; Van Bezu, J.; Van Hinsbergh, V. W. M.; Carman, C. V.; Brain, J. D.; Fredberg, J. J. et al. Substrate stiffening promotes endothelial monolayer disruption through enhanced physical forces. *Am. J. Physiol. Cell Physiol.* **2011**, *300*, C146–C154.

[12] Yi, B. C.; Yu, L.; Tang, H.; Wang, W. B.; Liu, W.; Zhang, Y. Z. Lysine-doped polydopamine coating enhances antithrombogenicity and endothelialization of an electrospun aligned fibrous vascular graft. *Appl. Mater. Today* **2021**, *25*, 101198.

[13] Ding, Y. H.; Yang, Z. L.; Bi, C. W. C.; Yang, M.; Xu, S. L.; Lu, X.; Huang, N.; Huang, P. B.; Leng, Y. Directing vascular cell selectivity and hemocompatibility on patterned platforms featuring variable topographic geometry and size. *ACS Appl. Mater. Interfaces* **2014**, *6*, 12062–12070.

[14] Govindarajan, T.; Shandas, R. Microgrooves encourage endothelial cell adhesion and organization on shape-memory polymer surfaces.

ACS Appl. Bio Mater. **2019**, *2*, 1897–1906.
[15] Chen, J. Y.; Hu, M.; Zhang, H.; Li, B. C.; Chang, H.; Ren, K. F.; Wang, Y. B.; Ji, J. Improved antithrombotic function of oriented endothelial cell monolayer on microgrooves. *ACS Biomater. Sci. Eng.* **2018**, *4*, 1976–1985.
[16] Sales, A.; Holle, A. W.; Kemkemer, R. Initial contact guidance during cell spreading is contractility-independent. *Soft Matter* **2017**, *13*, 5158–5167.
[17] Yi, B. C.; Xu, Q.; Liu, W. An overview of substrate stiffness guided cellular response and its applications in tissue regeneration. *Bioact. Mater.* **2022**, *15*, 82–102.
[18] Davis, G. E.; Senger, D. R. Endothelial extracellular matrix: Biosynthesis, remodeling, and functions during vascular morphogenesis and neovessel stabilization. *Circ. Res.* **2005**, *97*, 1093–1107.
[19] Taskin, M. B.; Ahmad, T.; Wistlich, L.; Meinel, L.; Schmitz, M.; Rossi, A.; Groll, J. Bioactive electrospun fibers: Fabrication strategies and a critical review of surface-sensitive characterization and quantification. *Chem. Rev.* **2021**, *121*, 11194–11237.
[20] Weekes, A.; Bartnikowski, N.; Pinto, N.; Jenkins, J.; Meinert, C.; Klein, T. J. Biofabrication of small diameter tissue-engineered vascular grafts. *Acta Biomater.* **2022**, *138*, 92–111.
[21] Sun, Q.; Hou, Y.; Chu, Z. Q.; Wei, Q. Soft overcomes the hard: Flexible materials adapt to cell adhesion to promote cell mechanotransduction. *Bioact. Mater.* **2022**, *10*, 397–404.
[22] Baker, B. M.; Trappmann, B.; Wang, W. Y.; Sakar, M. S.; Kim, I. L.; Shenoy, V. B.; Burdick, J. A.; Chen, C. S. Cell-mediated fibre recruitment drives extracellular matrix mechanosensing in engineered fibrillar microenvironments. *Nat. Mater.* **2015**, *14*, 1262–1268.
[23] Shin, Y. M.; Shin, H. J.; Heo, Y.; Jun, I.; Chung, Y. W.; Kim, K.; Lim, Y. M.; Jeon, H.; Shin, H. Engineering an aligned endothelial monolayer on a topologically modified nanofibrous platform with a micropatterned structure produced by femtosecond laser ablation. *J. Mater. Chem. B* **2017**, *5*, 318–328.
[24] Tang, H.; Yi, B. C.; Wang, X. L.; Shen, Y. B.; Zhang, Y. Z. Understanding the cellular responses based on low-density electrospun fiber networks. *Mat. Sci. Eng. C* **2021**, *119*, 111470.
[25] Berginski, M. E.; Gomez, S. M. The focal adhesion analysis server: A web tool for analyzing focal adhesion dynamics.. *F1000Res* **2013**, *2*, 68.
[26] Zhu, M. F.; Wu, Y. F.; Li, W.; Dong, X. H.; Chang, H.; Wang, K.; Wu, P. L.; Zhang, J.; Fan, G. W.; Wang, L. Y. et al. Biodegradable and elastomeric vascular grafts enable vascular remodeling. *Biomaterials* **2018**, *183*, 306–318.
[27] Sell, S. A.; McClure, M. J.; Garg, K.; Wolfe, P. S.; Bowlin, G. L. Electrospinning of collagen/biopolymers for regenerative medicine and cardiovascular tissue engineering. *Adv. Drug Deliver. Rev.* **2009**, *61*, 1007–1019.
[28] Meshel, A. S.; Wei, Q. Z.; Adelstein, R. S.; Sheetz, M. P. Basic mechanism of three-dimensional collagen fibre transport by fibroblasts. *Nat. Cell Biol.* **2005**, *7*, 157–164.
[29] Hansel, C. S.; Crowder, S. W.; Cooper, S.; Gopal, S.; Da Cruz, M. J. P.; Martins, L. D. O.; Keller, D.; Rothery, S.; Becce, M.; Cass, A. E. G. et al. Nanoneedle-mediated stimulation of cell mechanotransduction machinery. *ACS Nano* **2019**, *13*, 2913–2926.
[30] Soenen, S. J. H.; Nuytten, N.; De Meyer, S. F.; De Smedt, S. C.; De Cuyper, M. High intracellular iron oxide nanoparticle concentrations affect cellular cytoskeleton and focal adhesion kinase-mediated signaling. *Small* **2010**, *6*, 832–842.
[31] Mascharak, S.; Benitez, P. L.; Proctor, A. C.; Madl, C. M. ; Hu, K. H.; Dewi, R. E.; Butte, M. J.; Heilshorn, S. C. YAP-dependent mechanotransduction is required for proliferation and migration on native-like substrate topography.. *Biomaterials* **2017**, *115*, 155–166.
[32] Jiang, W. S.; Zhang, C. X.; Tran, L.; Wang, S. G.; Hakim, A. D.; Liu, H. N. Engineering nano-to-micron-patterned polymer coatings on bioresorbable magnesium for controlling human endothelial cell adhesion and morphology. *ACS Biomater. Sci. Eng.* **2020**, *6*, 3878–3898.
[33] Eguiluz, R. C. A.; Kaylan, K. B.; Underhill, G. H.; Leckband, D. E. Substrate stiffness and VE-cadherin mechano-transduction coordinate to regulate endothelial monolayer integrity. *Biomaterials* **2017**, *140*, 45–57.
[34] Wu, X. F.; Zhao, X. H.; Baylor, L.; Kaushal, S.; Eisenberg, E.; Greene, L. E. Clathrin exchange during clathrin-mediated endocytosis. *J. Cell Biol.* **2001**, *155*, 291–300.
[35] Qiao, D. H.; Yang, X. H.; Meyer, K.; Friedl, A. Glypican-1 regulates anaphase promoting complex/cyclosome substrates and cell cycle progression in endothelial cells. *Mol. Biol. Cell* **2008**, *19*, 2789–2801.
[36] Cancel, L. M.; Tarbell, J. M. The role of mitosis in LDL transport through cultured endothelial cell monolayers. *Am. J. Physiol. Circulat. Physiol.* **2011**, *300*, H769–H776.
[37] Ohashi, T.; Sato, M. Remodeling of vascular endothelial cells exposed to fluid shear stress: Experimental and numerical approach. *Fluid Dyn. Res.* **2005**, *37*, 40–59.
[38] Tzima, E.; Del Pozo, M. A.; Kiosses, W. B.; Mohamed, S. A.; Li, S.; Chien, S.; Schwartz, M. A. Activation of Rac1 by shear stress in endothelial cells mediates both cytoskeletal reorganization and effects on gene expression. *EMBO J.* **2002**, *21*, 6791–6800.
[39] Ng, D. H. J.; Humphries, J. D.; Byron, A.; Millon-Frémillon, A.; Humphries, M. J. Microtubule-dependent modulation of adhesion complex composition. *PLoS One* **2014**, *9*, e115213.
[40] Tedgui, A.; Mallat, Z. Anti-inflammatory mechanisms in the vascular wall. *Circ. Res.* **2001**, *88*, 877–887.
[41] Ciechanover, A.; Orian, A.; Schwartz, A. L. Ubiquitin-mediated proteolysis: Biological regulation via destruction. *Bioessays* **2000**, *22*, 442–451.
[42] Liu, L. J.; Michowski, W.; Kolodziejczyk, A.; Sicinski, P. The cell cycle in stem cell proliferation, pluripotency and differentiation. *Nat. Cell Biol.* **2019**, *21*, 1060–1067.
[43] Zachariae, W.; Tyson, J. J. Cell division: Flipping the mitotic switches. *Curr. Biol.* **2016**, *26*, R1272–R1274.
[44] Papakonstanti, E. A.; Vardaki, E. A.; Stournaras, C. Actin cytoskeleton: A signaling sensor in cell volume regulation. *Cell Physiol. Biochem.* **2000**, *10*, 257–264.
[45] Schnittler, H. J.; Schneider, S. W.; Raifer, H.; Luo, F.; Dieterich, P.; Just, I.; Aktories, K. Role of actin filaments in endothelial cell-cell adhesion and membrane stability under fluid shear stress. *Pfluger Arch.* **2001**, *442*, 675–687.
[46] Cunningham, K. S.; Gotlieb, A. I. The role of shear stress in the pathogenesis of atherosclerosis. *Lab. Invest.* **2005**, *85*, 9–23.
[47] Shen, Q.; Rigor, R. R.; Pivetti, C. D.; Wu, M. H.; Yuan, S. Y. Myosin light chain kinase in microvascular endothelial barrier function. *Cardiovasc. Res.* **2010**, *87*, 272–280.
[48] Tinsley, J. H.; De Lanerolle, P.; Wilson, E.; Ma, W. Y.; Yuan, S. Y. Myosin light chain kinase transference induces myosin light chain activation and endothelial hyperpermeability. *Am. J. Physiol. Cell Physiol.* **2000**, *279*, C1285–C1289.
[49] Lau, E. O. C.; Damiani, D.; Chehade, G.; Ruiz-Reig, N.; Saade, R.; Jossin, Y.; Aittaleb, M.; Schakman, O.; Tajeddine, N.; Gailly, P. et al. DIAPH3 deficiency links microtubules to mitotic errors, defective neurogenesis, and brain dysfunction. *eLife* **2021**, *10*, e61974.
[50] Gasiorowski, J. Z.; Liliensiek, S. J.; Russell, P.; Stephan, D. A.; Nealey, P. F.; Murphy, C. J. Alterations in gene expression of human vascular endothelial cells associated with nanotopographic cues. *Biomaterials* **2010**, *31*, 8882–8888.
[51] Vakifahmetoglu-Norberg, H.; Ouchida, A. T.; Norberg, E. The role of mitochondria in metabolism and cell death. *Biochem. Biophys. Res. Commun.* **2017**, *482*, 426–431.
[52] Rao, R. M.; Yang, L.; Garcia-Cardena, G.; Luscinskas, F. W. Endothelial-dependent mechanisms of leukocyte recruitment to the vascular wall. *Circ. Res.* **2007**, *101*, 234–247.
[53] Muller, W. A. Leukocyte–endothelial–cell interactions in leukocyte transmigration and the inflammatory response. *Trends Immunol.* **2003**, *24*, 326–333.
[54] Adams, R. H.; Eichmann, A. Axon guidance molecules in vascular patterning. *Cold Spring Harb Perspect. Biol.* **2010**, *2*, a001875.
[55] Kay, A. M.; Simpson, C. L.; Stewart, J. A.; Jr. The role of AGE/RAGE signaling in diabetes-mediated vascular calcification. *J.*

Diabetes Res. **2016**, *2016*, 6809703.
[56] Souilhol, C.; Serbanovic-Canic, J.; Fragiadaki, M.; Chico, T. J.; Ridger, V.; Roddie, H.; Evans, P. C. Endothelial responses to shear stress in atherosclerosis: A novel role for developmental genes. *Nat. Rev. Cardiol.* **2020**, *17*, 52–63.
[57] Bryant, J.; Ahern, D. J.; Brennan, F. M. CXCR4 and vascular cell adhesion molecule 1 are key chemokine/adhesion receptors in the migration of cytokine-activated T cells. *Arthritis Rheum.* **2012**, *64*, 2137–2146.
[58] Putney, J. W.; Tomita, T. Phospholipase C signaling and calcium influx. *Adv. Biol. Regul.* **2012**, *52*, 152–164.
[59] Thelen, M.; Stein, J. V. How chemokines invite leukocytes to dance. *Nat. Immunol.* **2008**, *9*, 953–959.
[60] Béliveau, É.; Guillemette, G. Microfilament and microtubule assembly is required for the propagation of inositol trisphosphate receptor-induced Ca2+ waves in bovine aortic endothelial cells. *J. Cell Biochem.* **2009**, *106*, 344–352.
[61] Wang, Z. H.; Liu, C. G.; Xiao, Y.; Gu, X.; Xu, Y.; Dong, N. G.; Zhang, S. M.; Qin, Q. H.; Wang, J. L. Remodeling of a cell-free vascular graft with nanolamellar intima into a neovessel. *ACS Nano* **2019**, *13*, 10576–10586.
[62] Liu, M.; Sun, A. Q.; Deng, X. Y. Numerical and experimental investigation of the hemodynamic performance of bifurcated stent grafts with various torsion angles. *Sci. Rep.* **2018**, *8*, 12625.
[63] Wang, Z. H.; Liu, C. G.; Zhu, D.; Gu, X.; Xu, Y.; Qin, Q. H.; Dong, N. G.; Zhang, S. M.; Wang, J. L. Untangling the co-effects of oriented nanotopography and sustained anticoagulation in a biomimetic intima on neovessel remodeling. *Biomaterials* **2020**, *231*, 119654.
[64] Song, K. H.; Kwon, K. W.; Song, S.; Suh, K. Y.; Doh, J. Dynamics of T cells on endothelial layers aligned by nanostructured surfaces. *Biomaterials* **2012**, *33*, 2007–2015.
[65] Wen, J. H.; Vincent, L. G.; Fuhrmann, A.; Choi, Y. S.; Hribar, K. C.; Taylor-Weiner, H.; Chen, S. C.; Engler, A. J. Interplay of matrix stiffness and protein tethering in stem cell differentiation. *Nat. Mater.* **2014**, *13*, 979–987.
[66] Kennedy, K. M.; Bhaw-Luximon, A.; Jhurry, D. Cell–matrix mechanical interaction in electrospun polymeric scaffolds for tissue engineering: Implications for scaffold design and performance. *Acta Biomater.* **2017**, *50*, 41–55.
[67] Liliensiek, S. J.; Wood, J. A.; Yong, J.; Auerbach, R.; Nealey, P. F.; Murphy, C. J. Modulation of human vascular endothelial cell behaviors by nanotopographic cues. *Biomaterials* **2010**, *31*, 5418–5426.
[68] Fu, Y.; Xiao, S. H.; Hong, T. T.; Shaw, R. M. Cytoskeleton regulation of ion channels. *Circulation* **2015**, *131*, 689–691.
[69] Jain, A.; Graveline, A.; Waterhouse, A.; Vernet, A.; Flaumenhaft, R.; Ingber, D. E. A shear gradient-activated microfluidic device for automated monitoring of whole blood haemostasis and platelet function. *Nat. Commun.* **2016**, *7*, 10176.
[70] Baeyens, N.; Schwartz, M. A. Biomechanics of vascular mechanosensation and remodeling. *Mol. Biol. Cell* **2016**, *27*, 7–11.
[71] Gerhold, K. A.; Schwartz, M. A. Ion channels in endothelial responses to fluid shear stress. *Physiology (Bethesda)* **2016**, *31*, 359–369.
[72] Ali Shahzad, K.; Qin, Z. J.; Li, Y.; Xia, D. L. The roles of focal adhesion and cytoskeleton systems in fluid shear stress-induced endothelial cell response. *Biocell* **2020**, *44*, 137–145.